Engineering Structures 247 (2021) 113229

Contents lists available at ScienceDirect

Engineering Structures

journal homepage: www.elsevier.com/locate/engstruct

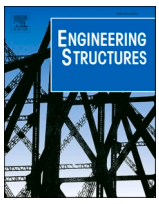

First mode damping ratio oriented optimal design procedure for damped outrigger systems with additional linear viscous dampers

Tomoki Asai [a], Yuki Terazawa [a,*], Takashi Miyazaki [b], Pao-Chun Lin [c], Toru Takeuchi [a]

[a] Tokyo Institute of Technology, Ookayama 2-12-1, Meguro-ku, Tokyo 152-8550, Japan
[b] Nippon Steel Engineering, Ohsaki 1-5-1, Shinagawa-ku, Tokyo 141-8604, Japan
[c] National Cheng Kung University, Department of Civil Engineering, Tainan, Taiwan

ARTICLE INFO

Keyword:
Damped outrigger system
Linear viscous damper
Optimal design
Complex eigenvalue analysis
Machine learning
Response spectrum analysis

ABSTRACT

The damped outrigger system is in widespread use as a damping modification system for tall buildings that provides high additional damping in addition to the bending back effect against the core. However, while the enhanced seismic performance of damped outrigger systems was confirmed in previous studies all over the world, a general-purpose optimal design method focusing on modal damping ratios has not been established yet. This paper proposes an optimal damper design kit composed of a first mode damping ratio oriented design policy, simple equations of optimal damper-connection stiffness ratio to maximize first mode damping ratio, a machine learning model to estimate first mode natural period and damping ratio. The tenability of the first mode damping ratio-oriented design policy was confirmed by performing complex modal analyses on single to quad damped outrigger systems incorporating linear viscous dampers and assigning realistic stiffness values to the outrigger trusses. The simple design equations of optimal damper-connection stiffness ratio and the machine learning model for first mode characteristics were developed based on a large number of analytical results. The proposed optimal design kit has been made available as a web application-based design tool.

1. Introduction

The outrigger system is a structural system for tall buildings wherein a rigid core at the center is connected to the perimeter columns via outriggers. As shown in Fig. 1(a), the column-restrained outrigger resists the flexural response of the core to reduce the story drift and overturning moment[12]. Smith and Willford [3] proposed a damped outrigger system (Fig. 1(b)), in which seismic energy dissipation devices (i.e., dampers) are inserted between the outrigger and the perimeter column. The dampers provide additional damping by operating on the relative vertical motion between the perimeter column and the outrigger during flexure. These types of damped outrigger systems are being widely used to design tall buildings in windy and seismic regions such as the United States, China, and the Philippines [4]. Smith and Willford suggested the importance of focusing on modal damping ratios at the design stage to mitigate both the seismic and wind response [3,5]. It was concluded that to find the optimal damping coefficient (C_{opt}) for optimal design, it is also necessary to assume some cases where the design cannot be done using C_{opt} for reasons such as economic efficiency. However, a general-purpose optimal design method focusing on modal damping ratios has not been established yet while the enhanced seismic performance of damped outrigger systems is confirmed in previous studies all over the world.

Chen et al. [6] developed a theoretical model for a damped outrigger system incorporating viscous dampers based on the continuum beam theory and calculated the modal damping ratios from complex eigenvalue analysis. However, the scope of this theoretical model was limited to the case when both the outrigger truss and perimeter columns are rigid. Similar theoretical models to Chen et al. were proposed by Deng et al. [7] and Zhou et al. [8]. Tan et al. [9] also studied the optimal design variables (i.e., the outrigger height and the damping coefficient) using the theoretical models [6]. Huang et al. [10] developed a theoretical model considering the stiffness of outrigger and perimeter columns and proposed a design equation to obtain the optimal design variables maximizing the damping ratio of the first mode. However, the design equation was formulated based on unrealistic models with very stiff outrigger trusses and its application was limited to single damped outrigger systems.

* Corresponding author.
E-mail addresses: asai.t.ae@m.titech.ac.jp (T. Asai), terazawa.y.aa@m.titech.ac.jp (Y. Terazawa), miyazaki.takashi.pr6@eng.nipponsteel.com (T. Miyazaki), pclin@gs.ncku.edu.tw (P.-C. Lin), takeuchi.t.ab@m.titech.ac.jp (T. Takeuchi).

https://doi.org/10.1016/j.engstruct.2021.113229
Received 7 May 2021; Received in revised form 30 August 2021; Accepted 14 September 2021
Available online 25 September 2021

Although these studies have all focused on modal damping ratios, the relationship between the modal damping ratios and their effects on seismic response reduction were not discussed in detail. Lin et al. [12 13] analyzed the relationship between the outrigger height, the yielding force and the seismic response reduction for single and dual outrigger systems incorporating buckling-restrained braces, and proposed an optimal design guideline to mitigate a specific kind of seismic response. However, since non-linear response history analysis was mainly used, the exact non-proportional modal damping ratios were not discussed. The optimal design guidelines were developed based on the response of analytical models with very stiff outrigger trusses, and the applicability of those guidelines to practical design is uncertain. Terazawa et al. [14] also conducted a similar study for a single damped outrigger with viscous dampers. Morales et al. [12] analyzed the dynamic characteristics of a specific dual damped outrigger system but the optimal design method was beyond the scope of the study.

Structural design engineers in areas of high seismic hazard are expected to design the damped outrigger systems such that I) the design constraints of the building plan (i.e., the location of the outrigger layer or the outrigger length, and being open to sudden plan changes) are adhered to and II) the damping ratio provided is high while ensuring that III) the system is economical (i.e., the damping coefficient is not unreasonably high), IV) the seismic response is within limits and V) the design is flexible to accommodate any changes in plans. Therefore, it is necessary to provide a generalized design procedure that enables the engineer to design the system adhering to these requirements. It is also necessary to provide a simple and efficient approach to estimate the required damping coefficient and dynamic response characteristics according to rapidly changing plans. For this purpose, it is necessary to rearrange the exact dynamic response characteristics by applying complex modal analysis to discrete framing models.

Based on the literature review, the novel objectives of this study are 1) to investigate further the relationship between the exact modal characteristics of linear damped outrigger systems and the seismic response reduction effects by performing response spectrum analyses using practical (realistic) building models, 2) to conduct parametric studies to propose a first mode damping ratio oriented optimal design policy, and 3) to propose a web application-based design tool composed of both the simple design equations to maximize the first mode damping ratio for linear damped outrigger systems and the machine learning models to estimate the first mode characteristics of any arbitrary linear damped outrigger system. In Section 2, the numerical models and analysis method are described and the main design variables of the damped outrigger system are defined. In Section 3, the fundamental relationship between the design variables, the modal characteristics, and seismic response reduction effects are briefly reviewed for a single damped outrigger system, and a design policy maximizing the first mode damping ratio is proposed. The applicability of the optimal outrigger height ratio proposed by Lin et al. [12] is also discussed. In Section 4, the optimal outrigger height ratios, optimal damping coefficients, and optimal damper-to-connection stiffness ratios for dual damped outrigger systems are analyzed in detail, and the validity of the design policy is verified. The second mode damping ratio-oriented design approach is also discussed. In Section 5, the upper limit of the first mode damping ratio increased by damped outriggers is verified by increasing the number of outriggers. In Section 6, simple design equations of optimal damper-to-connection stiffness ratio to maximize first mode damping ratio, and a machine learning model to estimate first mode period and first mode damping ratio are developed. Finally, a web application-based optimal design tool incorporating these design equations is presented, and its application is outlined using a design example. Numerous dampers including fluid viscous dampers, bilinear oil dampers, viscoelastic dampers as discussed in [15–17], friction dampers, elasto-plastic dampers such as the buckling-restrained braces [18] are available for employment in damped outrigger systems. However, this paper focuses on damped outrigger systems incorporating only linear viscous dampers where the modal characteristics are independent of the seismic input, and nonlinear dampers based systems are in future work[19].

2. Numerical analysis

2.1. Numerical model and parameter definition

A numerical model was constructed (Fig. 2(a) and 2(b)) assuming a typical damped outrigger structure which consists of a pin-jointed column-beam frame to support the vertical loads, a central core to resist the horizontal loads, outriggers, and linear viscous dampers. This member-by-member planar model was further simplified to a discrete mass model (DM model [12]) for the parametric study as shown in Fig. 2(c). This DM model consists of truss elements simulating the perimeter columns, beam elements simulating the core and outriggers, and linear dashpots simulating the linear viscous dampers. As shown in the enlarged part of Fig. 2(c), while the perimeter columns are modeled as single elements, the core and outriggers have intermediate nodes to simulate higher mode deformation. The horizontal displacement of the top of the perimeter columns was kept equal to the horizontal displacement of the outrigger to prevent an anomalous vibration mode. For the sake of simplicity, uniform cross-sections are assigned to the perimeter columns and the core. The validity of the DM model against the full model for the seismic response was verified in the previous study [12].

The design variables of single and dual damped outrigger models are summarized in Fig. 3. Here, h is the building height, l_t is the outrigger span, EI is the flexural stiffness of the core, i is the i-th outrigger layer

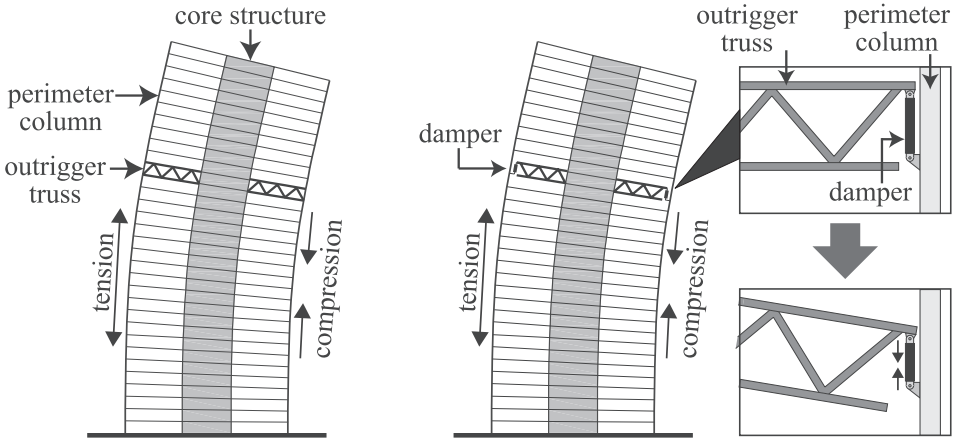

Fig. 1. Mechanism of outrigger system.

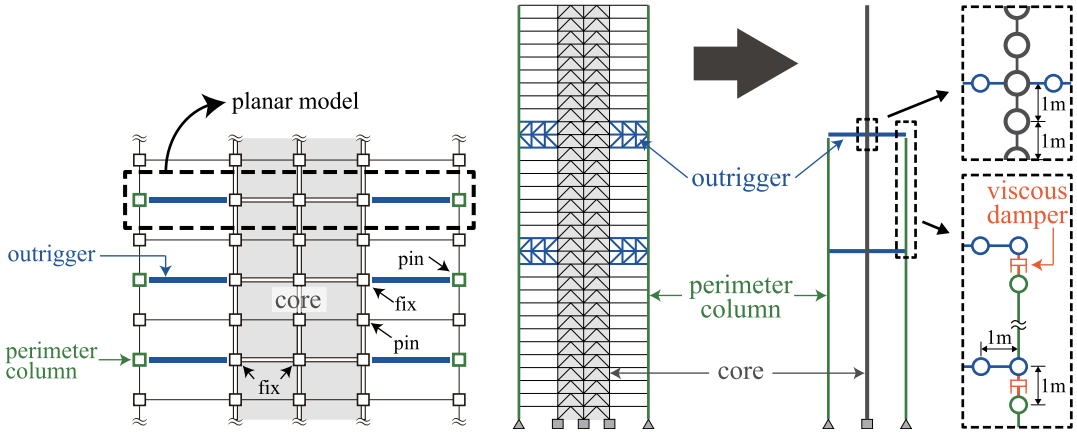

Fig. 2. Schematic image of the numerical model.

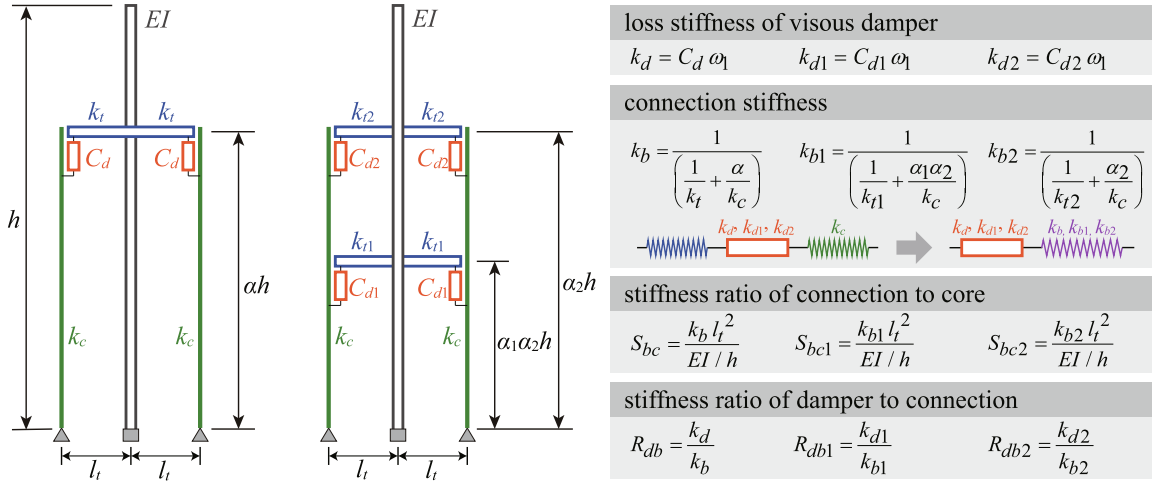

Fig. 3. Schematic image explaining the design variables.

from the base, α and α_i are the outrigger height ratios, k_t and k_{ti} are the flexural stiffness of the outrigger, k_c is the axial stiffness of the perimeter column ($\alpha_i = 1.0$) and k_c/α_i is the axial stiffness of the perimeter column corresponding the i-th outrigger layer. Further, as shown in Fig. 3(c), the damper stiffness k_{di} is defined as the product of C_{di} which represents the amount of viscous damper and the first mode natural circular frequency ω_1 of the bare core model. The flexural stiffness of the outrigger may be assumed to be the same as that of the perimeter column and the damper in the vertical direction. Therefore, the "connection stiffness k_{bi}" is computed by combining the stiffness of the perimeter column and the outrigger as shown in Fig. 3. S_{bci} is the stiffness ratio between the core and the connection and R_{dbi} ($=k_{di}/k_{bi}$) is the damper-connection stiffness ratio.

The building specifications are shown in Fig. 4, and the details of the numerical models for the parametric study are listed in Table 1. The story height is 4 m and the building heights (h) of the 16-story model, the 32-story model, the 64-story model, and the 96-story model are 64 m, 128 m, 256 m, 384 m, respectively. The dead load is about 0.8 ton/m^2, which is assigned to the nodes in the core. The flexural stiffness EI of the core is designed so that the first mode natural period is about 0.03 hs and the flexural stiffness of the 16-story model, the 32-story model, the 64-story model, and the 96-story model are 1.09×10^9 kNm^2, 5.17×10^9 kNm^2, 2.79×10^{10} kNm^2, and 7.05×10^{10} kNm^2, respectively. The perimeter columns are designed using allowable stress design principle to satisfy a demand capacity ratio of 0.5 under the long-term dead load, and CFT-600*25, CFT-800*36, CFT-1000*50, and CFT-1300*50 are assigned to the 16-story model, the 32-story model, the 64-story model, and the 96-story model, respectively. As concrete is weak in tension, the axial stiffness k_c of the perimeter column is derived only from the steel pipe of the CFT column, and the resulting axial stiffness of the 16-story model, the 32-story model, the 64-story model, and the 96-story model is 1.84×10^5 kN/m, 1.76×10^5 kN/m, 1.52×10^5 kN/m, 1.33×10^5 kN/m, respectively. Outrigger span l_t is 12 m for the 16-story model and the 32-story model, and is 16 m for the 64-story model and the 96-story model, considering the rentable ratio. Three different flexural stiffness of the outriggers (0.5×10^6 kN/m, 0.25×10^6 kN/m, and 1.0×10^6 kN/m) are considered, and k_t equal to 0.5×10^6 kN/m of corresponds to the regular (practical) outrigger truss shown in Fig. 4. In the previous studies [10–14], the flexural stiffness of the outrigger was an order of magnitude larger than the stiffness values in practice, and hence the numerical analysis results are not necessarily realistic. The parameters corresponding to the damping coefficient (listed in Table 1) increase in proportion to the building height h. The outrigger height ratio α_i – the core-to-connection stiffness ratio S_{bci} relationship is shown in Fig. 5 (a) and Fig. 5 (b), and the outrigger height ratio α_i – the damper-connection stiffness ratio R_{dbi} are shown in Fig. 5(c) and Fig. 5(d). The parameters S_{bci} and R_{dbi} are explicitly determined from the model parameters shown in Fig. 3, and vary depending on the outrigger stiffness k_t and the outrigger height α as discussed later in the parametric study.

2.2. Analysis methods and input ground motions

Complex eigenvalue analysis, linear response history analysis (LRHA), and generalized response spectrum analysis [20,21] (GRSA)

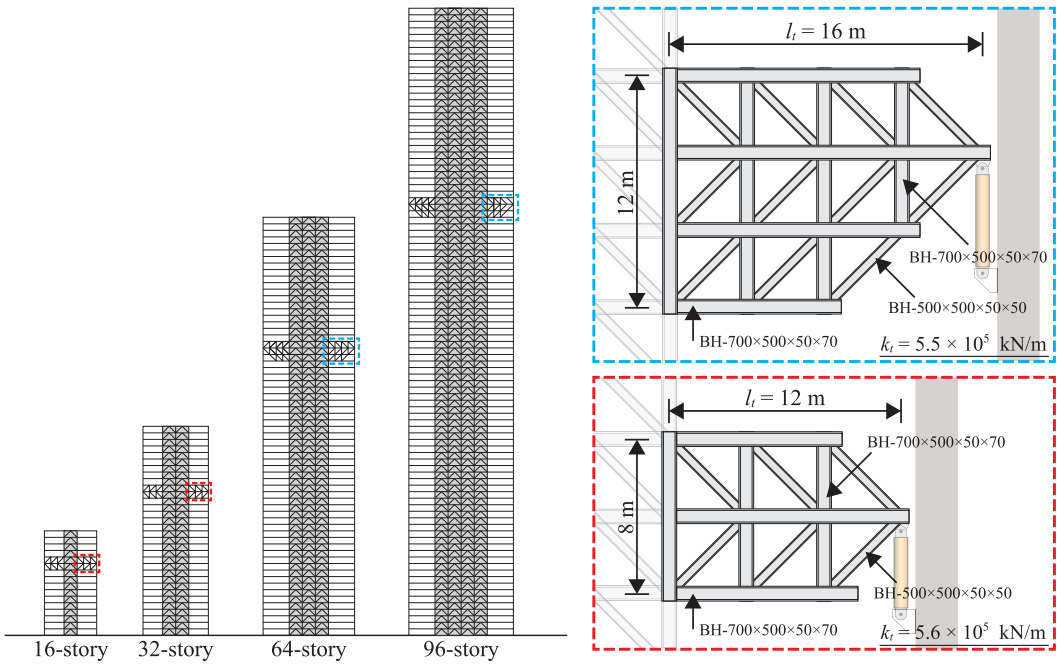

(a) Flaming plan

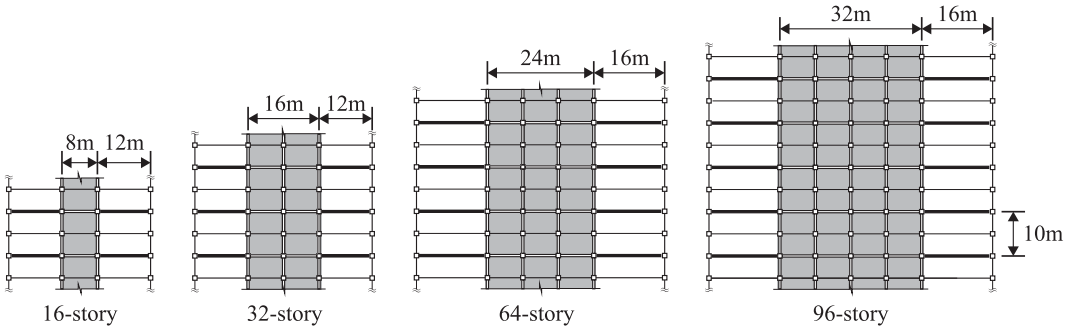

(b) Floor plan

Fig. 4. Building specifications.

Table 1
Numerical model data.

Story	Building height h (m)	Flexural stiffness of the core EI (kNm^2)	Axial stiffness of the perimeter column k_c (kN/m)	Outrigger Span l_t (m)	Flexural stiffness of the outrigger k_{ti} (kN/m)	Damping coefficient of the damper C_{di} (kN-s/mm)
16	64	1.09 × 10^9	1.84 × 10^5	12	0.25 × 10^6	10–70
32	128	5.17 × 10^9	1.76 × 10^5		0.5 × 10^6	20–140
64	256	2.79 × 10^{10}	1.52 × 10^5	16	1.0 × 10^6	40–280
96	384	7.05 × 10^{10}	1.33 × 10^5			60–420

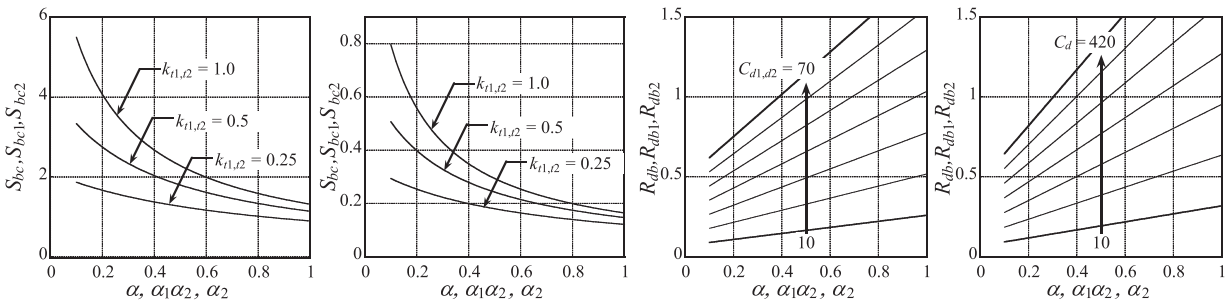

(a) S_{bc} - α (16-story) (b) S_{bc} - α (96-story) (c) R_{db} - α (16-story) (d) R_{db} - α (96-story)

Fig. 5. S_{bci} _ α_i relationship and R_{dbi} _ α_i relationship.

were performed on the analytical models.

Complex eigenvalue analysis is used to calculate modal characteristics of non-proportional damping systems considering dampers. LRHA is used to verify the accuracy of GRSA. The Newmark method ($\beta = 1/4$) is used to calculate the incremental displacement. The Rayleigh-type proportional damping matrix is adopted, and the first and second mode's initial damping ratios are set to 2%.

GRSA is used to analyze the modal seismic response. GRSA is a series of numerical analyses which iteratively performs complex eigenvalue analysis and response spectrum analysis, and was developed to quickly evaluate the dynamic characteristics of a structural analysis model with finite linear or nonlinear dampers in the extensive parametric study. While the equivalent modal characteristics of the model with nonlinear dampers and the maximum seismic response can be evaluated from the iterative computation using the substitute model with equivalent linearized damping element, the seismic response of the model with only linear viscous dampers is directly evaluated from the initial complex eigenvalue analysis results. The evaluation procedure is briefly described as follows.

After the initial complex eigenvalue analysis results are obtained, the maximum seismic response is calculated from the complete quadratic combination rule for non-proportional damping systems (the modified CQC rule proposed by Sinha and Igusa [22]) shown in Eq. (1),

$$R_{\mathrm{CQC}} = \sqrt{\sum_{s=1}^{n}\sum_{r=1}^{n} B_s B_r S_s(\omega_s,\xi_s) S_r(\omega_r,\xi_r) cos(\theta_s-\theta_r)\rho_{sr}}. \quad (1)$$

where n is the number of modes required to achieve modal mass participation of over 90%, s and r are mode numbers, ξ is the modal damping ratio, ρ is the correlation coefficient of the various modes, ω is the natural circular frequency, S is the response spectrum value, $B = |\mathrm{Re}(\lambda^*\beta\varphi)/\sin(\theta)|$, $\theta = \tan^{-1}(-\mathrm{Re}(\lambda^*\beta\varphi)/\mathrm{Re}(\beta\varphi))$, λ is the complex eigenvalue, β is the complex stimulus coefficient, φ is the complex eigenvector component, * is the complex conjugate.

In GRSA, the response spectrum values of the representative damping ratio ($\xi_0 = 1, 2, 3, 5, 10, 15, 20, 30\%$) are given beforehand from an external file, and the response spectrum value of the arbitrary damping ratio ξ, which is used in Eq. (1), are calculated by multiplying the response spectrum value of the closest ξ_0 with the response reduction effect factor D_h [23] shown in Eq. (2),

$$\begin{aligned} D_h &= (D_{h0}-1)(5T)+1 && (0.0s \leqslant T < 0.2s) \\ D_h &= D_{h0} && (0.2s \leqslant T < 2.0s) \\ D_h &= D_{h0}\{\sqrt{\xi/\xi_0}(T-2)/40+1\} && (2.0s \leqslant T < 8.0s) \end{aligned} \quad (2)$$

where $D_{h0} = \sqrt{(1+25\xi_0)/(1+25\xi_i)}$.

Three Japanese spectrally matched seismic waves [24] (El Centro, Hachinohe, JMA Kobe) and one artificial wave KA1 (as an example of a long period wave [25]) considering the soil structure of Tokyo are assigned. The acceleration response spectra and displacement response spectra are shown in Fig. 6.

Comparisons between LRHAs and GRSAs are summarized in Fig. 7. As shown in Fig. 7, the errors between LRHAs and GRSAs are within 20% for each of the three seismic response parameters.

3. Optimal design variable values of single damped outrigger system

3.1. First mode natural period and first mode damping ratio

An example demonstrating the relationship between the first four modal characteristics and the outrigger height ratio α for the 64-story model ($k_t = 0.5 \times 10^6$ kN/m, and $C_d = 200$ kN-s/mm) are shown in Fig. 8. In the case of the bare core model and the fixed model, where the perimeter columns are directly connected to the outrigger truss, α had a large influence on the first mode's period but had a negligible influence on the period of the higher modes. Furthermore, the first mode's additional damping ratio varies greatly with α, while the higher modes' damping ratio exhibited lesser variation (Fig. 8(b)). This tendency arises as the first mode is predominant in the relative velocity response of the damper element in single damped outrigger systems. This implies that the single damped outrigger system shows a strong dependence on the first modal characteristics and is therefore effective in controlling the first mode response. In previous studies, the higher mode's additional damping ratios were also observed to increase with α in single damped outrigger systems where the damped outrigger is considered as a damped rotational spring [6], and the present study's exact complex eigenvalue analysis results suggest that the trend from the previously studied theoretical models were not accurate.

The relationship between the first mode characteristics and α for all models are shown in Fig. 9. It may be seen that the larger the C_d, the lower the optimum α, and the smaller the C_d, the higher the optimum α. As shown in Fig. 9(a), the first mode's natural period decreases as the damped outrigger is added to the core model increasing C_d and eventually converges to the period of the fixed model. The first mode period is at a minimum when α is 0.7. As shown in Fig. 9(b), the first mode damping ratio increases with C_d, reaches a maximum and then decreases. This suggests that when C_d is increased, the deformation of the connection becomes more than that of the damper. The first modal damping ratio is maximum at $\alpha = 0.6$, which is slightly lower than the optimal α minimizing the first mode period. This is because it is necessary to ensure a higher k_c/α for a higher damping ratio. The first mode damping ratio is maximum when C_d is approximately 120 kN-s/mm.

3.2. Seismic response

The relationship between the seismic response parameters and α are

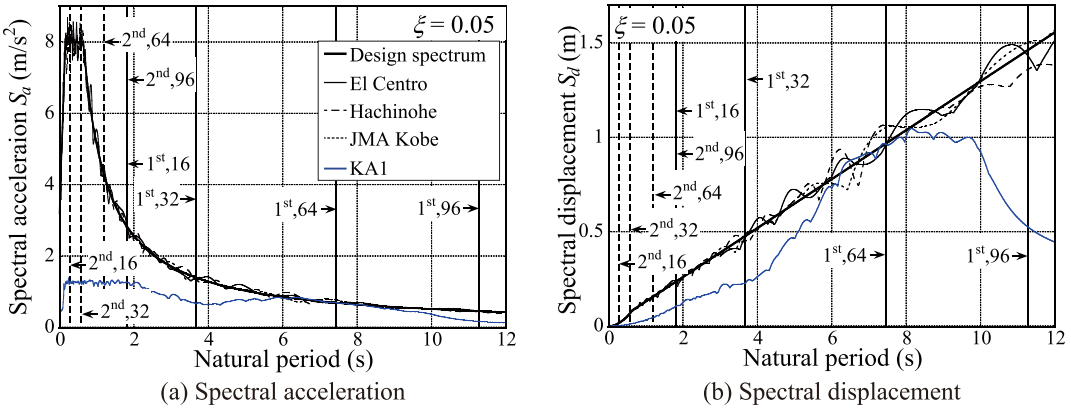

(a) Spectral acceleration (b) Spectral displacement

Fig. 6. Response spectra.

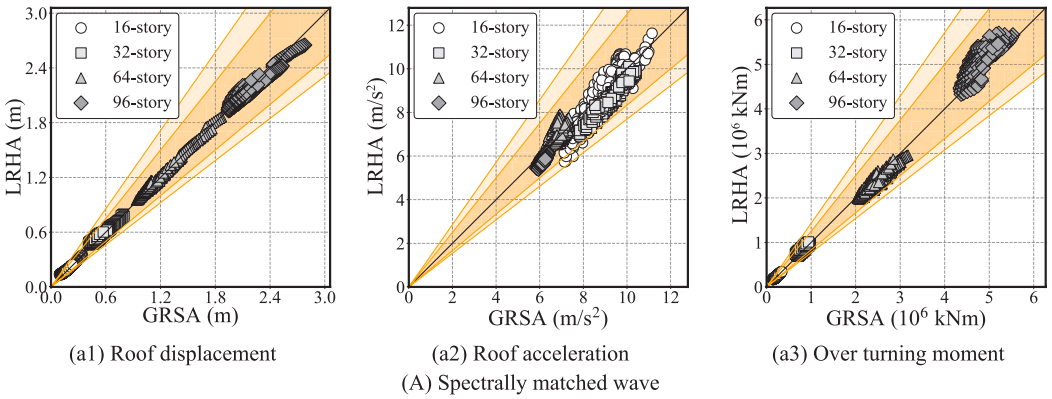

Fig. 7. Comparison of LRHA and GRSA response ($k_{t1} = k_{t2} = 0.5 \times 10^6$ kN/m).

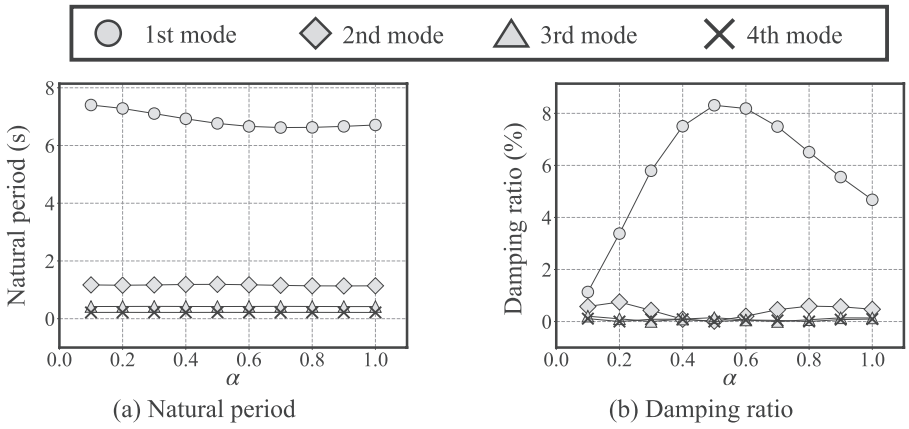

Fig. 8. First to fourth mode characteristics of single damped outrigger models (64-story, $k_t = 0.5 \times 10^6$ kN/m, $C_d = 200$ kN-s/mm).

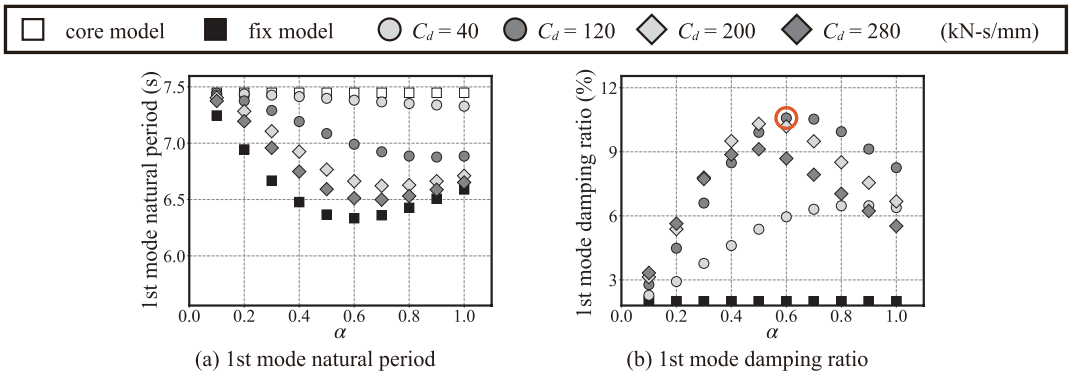

Fig. 9. Modal characteristics of single damped outrigger models ($k_t = 0.5 \times 10^6$ kN/m, 64-story).

shown in Fig. 10. All seismic response parameters reduce with increasing damping ratio as shown in Figs. 8(b) and 9(b). Optimal outrigger height ratio α_{opt} to minimize the roof displacement is 0.6, the story drift ratio is 0.8, the roof acceleration is 0.9 and the overturning moment is 0.7 respectively. Compared with the α_{opt} value that minimizes the first mode characteristics, these α_{opt} values form a wider range but follow the former trend of larger the C_d, the lower the optimum α, and the smaller the C_d, the higher the optimum α as discussed in Section 3.1. The optimal C_{dopt} that minimizes the roof acceleration is about 40 kN-s/mm and is 200 kN-s/mm for other response parameters. Nevertheless, as shown in the orange marker, for cases when the first mode damping ratio is maximum (shown in Fig. 9(b)), the seismic response reduced significantly although the reduction in roof acceleration is comparatively lesser than those observed for other parameters. This validates the effectiveness of maximizing the first mode damping ratio in the single damped outrigger system and is therefore adopted as a design guideline.

3.3. Summary and comparison of results with previous studies

The modal characteristics, reduction ratios of seismic responses and the summary of optimal values of α, C_d, R_{db} are listed in Table 2. The optimal values obtained from the previous numerical studies are also listed in Table 2(d). The larger the k_t, the shorter the natural period, the higher the damping ratio, and the smaller the seismic response. Therefore, it is desirable to design k_t as large as possible because it is common

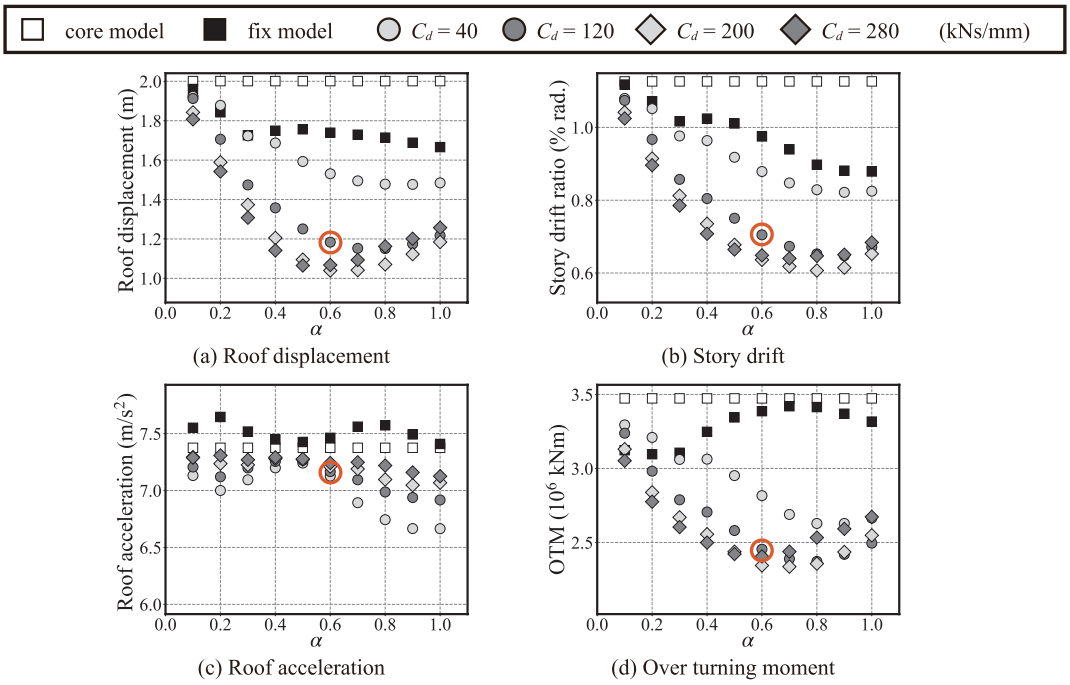

Fig. 10. Seismic response of single damped outrigger models ($k_t = 0.5 \times 10^6$ kN/m, 64-story).

Table 2
Summary of the optimal values for the single damped outrigger models.

	Story	value	Optimal value			value	Optimal value			value	Optimal value			value	Optimal value		
			α	C_d	R_{db}		α	C_d	R_{db}		α	C_d	R_{db}		α	C_d	R_{db}
First mode natural period	16	1.29	0.6	N/A	N/A	1.21	0.6	N/A	N/A	1.15	0.55	N/A	N/A	0.94	0.5	N/A	N/A
	32	3.08	0.65	N/A	N/A	2.98	0.65	N/A	N/A	2.91	0.65	N/A	N/A	2.28	0.5	N/A	N/A
	64	6.64	0.7	N/A	N/A	6.50	0.7	N/A	N/A	6.41	0.65	N/A	N/A	5.31	0.5	N/A	N/A
	96	10.52	0.7	N/A	N/A	10.40	0.7	N/A	N/A	10.33	0.7	N/A	N/A	N/A	N/A	N/A	N/A
First mode damping ratio	16	23	0.6	20	0.51	28	0.55	25	0.43	32	0.5	30	0.39	42	0.6	65	0.28
	32	12	0.65	50	0.66	16	0.6	70	0.65	18	0.55	80	0.56	28	0.5	221	0.45
	64	9	0.65	120	0.84	11	0.6	140	0.70	12	0.55	180	0.70	17	0.5	577	0.60
	96	6	0.65	180	0.89	7	0.6	240	0.87	8	0.55	270	0.77	N/A	N/A	N/A	N/A
Roof displacement (RD)	16	71	0.65	30	0.79	75	0.6	35	0.64	79	0.6	40	0.59	84	0.5	95	0.35
	32	42	0.65	70	0.92	48	0.65	120	1.17	52	0.6	130	0.98	68	0.6	300	0.70
	64	42	0.7	200	1.45	48	0.65	200	1.06	51	0.6	200	0.83	55	0.6	577	0.70
	96	23	0.7	180	0.93	27	0.6	270	0.98	30	0.6	300	0.92	N/A	N/A	N/A	N/A
Story drift ratio (SD)	16	73	0.75	25	0.70	77	0.7	30	0.61	79	0.65	35	0.55	84	0.6	95	0.40
	32	44	0.85	120	1.81	49	0.8	90	1.01	53	0.8	110	1.04	68	0.7	221	0.59
	64	40	0.85	180	1.46	46	0.85	200	1.28	49	0.85	180	1.00	53	0.8	577	0.90
	96	22	0.85	180	1.04	26	0.8	240	1.07	28	0.8	270	1.05	N/A	N/A	N/A	N/A
Roof acceleration (RA)	16	33	0.9	10	0.31	36	0.95	10	0.25	37	0.9	10	0.20	52	0.9	50	0.28
	32	16	1	20	0.33	19	0.9	20	0.24	21	0.9	20	0.21	46	0.9	116	0.37
	64	8	0.95	40	0.35	10	0.95	40	0.28	11	0.95	40	0.24	20	0.9	223	0.37
	96	3	0.95	60	0.37	4	0.95	60	0.31	4	0.95	60	0.27	N/A	N/A	N/A	N/A
Base shear (BS)	16	46	0.8	10	0.29	50	0.75	10	0.21	52	0.75	10	0.18	59	0.7	36	0.17
	32	23	0.85	20	0.30	27	0.85	20	0.23	30	0.85	20	0.20	47	0.8	116	0.34
	64	16	0.85	40	0.32	19	0.85	40	0.26	21	0.85	40	0.22	25	0.9	123	0.19
	96	8	0.85	60	0.35	10	0.85	60	0.28	11	0.85	60	0.25	N/A	N/A	N/A	N/A
Over turning moment (OTM)	16	-58	0.6	30	0.76	-61	0.6	30	0.55	-66	0.25	70	0.57	-78	0.1	757	0.60
	32	-33	0.7	40	0.55	-36	0.7	40	0.41	-38	0.75	40	0.36	-55	0.2	826	0.70
	64	-28	0.7	160	1.16	-33	0.65	200	1.06	-36	0.75	180	0.90	-41	0.7	324	0.45
	96	-15	0.75	150	0.81	-18	0.75	150	0.64	-20	0.75	180	0.66	N/A	N/A	N/A	N/A

※ units: natural period (s); the damping ratio (%) and the seismic response reduction ratio (%).

to have a higher degree of design freedom in k_t than k_c. The optimal value of α depends on the height, k_t and the objective functions, but is mostly in the range of 0.5–0.9. This range is similar to, albeit slightly larger than the results presented in Lin et al. [12]. The optimal value of C_d increases with k_t. (Note that k_t was very large in the previous study). It also increases with the building height and depends greatly on the objective functions. The optimal value of R_{db} increases with building height and decreasing k_t. This trend is the same as that observed by Lin et al. [12] wherein the optimal R_{db} value decreased with an increase in the S_{bc}. The optimal R_{db} value depends greatly on the objective

functions, and is in the range of 0.2–0.4 when the roof acceleration and the base shear are minimized. The obtained optimal value is in the range of 0.4–0.9 when the first mode damping ratio is maximized and is in the range of 0.6–1.0 when minimizing the seismic response. In summary, the trends of dynamic characteristics and optimal values of α, C_d, R_{db} in this study are generally consistent with those of previous studies even though the studied analytical ranges are significantly different.

4. Optimal design variable values of dual damped outrigger system

4.1. Optimal outrigger height ratio for first and second mode characteristics

This section investigates the optimal outrigger height ratio based on the first and second modal characteristics in a dual damped outrigger system. The relationship between the first mode natural period, first mode damping ratio, second mode damping ratio and design variables are shown in Fig. 11. The horizontal axis title β is defined in Eq. (3), where the i-th decimal place corresponds to α_i.

$$\beta = \sum_{i=1}^{n} 10^{i-n}\alpha_i \;=\; \alpha_2 + 0.1\,\alpha_1 \;(n = 2,\ \text{dual outrigger}). \tag{3}$$

For example,$\beta = 0.75$ means the dual outrigger positions with $\alpha_1 = 0.5$ and $\alpha_2 = 0.7$.

As shown in Fig. 11(a), adding a lower outrigger to the single damped outrigger (period equal to 6.6 s) reduces the first mode natural period to about 6.3 s. The optimal range for the outrigger height ratio α_2 was found to be 0.7–0.8 and for α_1 was around 0.6–0.7, which are slightly larger than the corresponding optimal α values for the single damped outrigger (=0.7). These optimal outrigger height ratios are comparable to those observed in Lin et al.'s study using BRB [13]. However, the method presented in this paper allows for a more detailed and comprehensive analysis of the effect of the multiple outriggers on the higher mode response. As shown in Fig. 11(b), by adding a damped outrigger below the single damped outrigger, the first mode damping ratio increases from 10.5% to 13%. However, for cases when the damping coefficient is large ($C_{d1} = C_{d2} = 200$ kN-s/mm) and the outrigger spacing is close ($\alpha_1 \geq 0.7$), the first mode damping ratio is lower than that of the single damped outrigger. The optimal ranges obtained for outrigger height ratios α_2 and α_1 are 0.6–0.7 and 0.5–0.6 respectively, which are slightly lower than the optimal α_1, α_2 ranges obtained from minimising the first mode natural period. This suggests that it is necessary to ensure a high value of k_c/α to achieve a higher damping ratio as was in the case of a single damped outrigger. As shown in Fig. 11(c), adding a lower damped outrigger to a single damped outrigger increases the second mode damping ratio from 4% to about 7%. This suggests that dual damped outriggers are more effective than single outriggers in controlling the higher second mode response. However, when the damping coefficient is large ($C_{d1} = C_{d2} = 200$ kN-s/mm) and the outrigger spacing is close ($\alpha_1 \geq 0.7$), the second mode's damping ratio is lower than that of the single damped outrigger. The optimal ranges for outrigger height ratios α_2 and α_1 are 0.8–0.9 and 0.2–0.3 respectively.

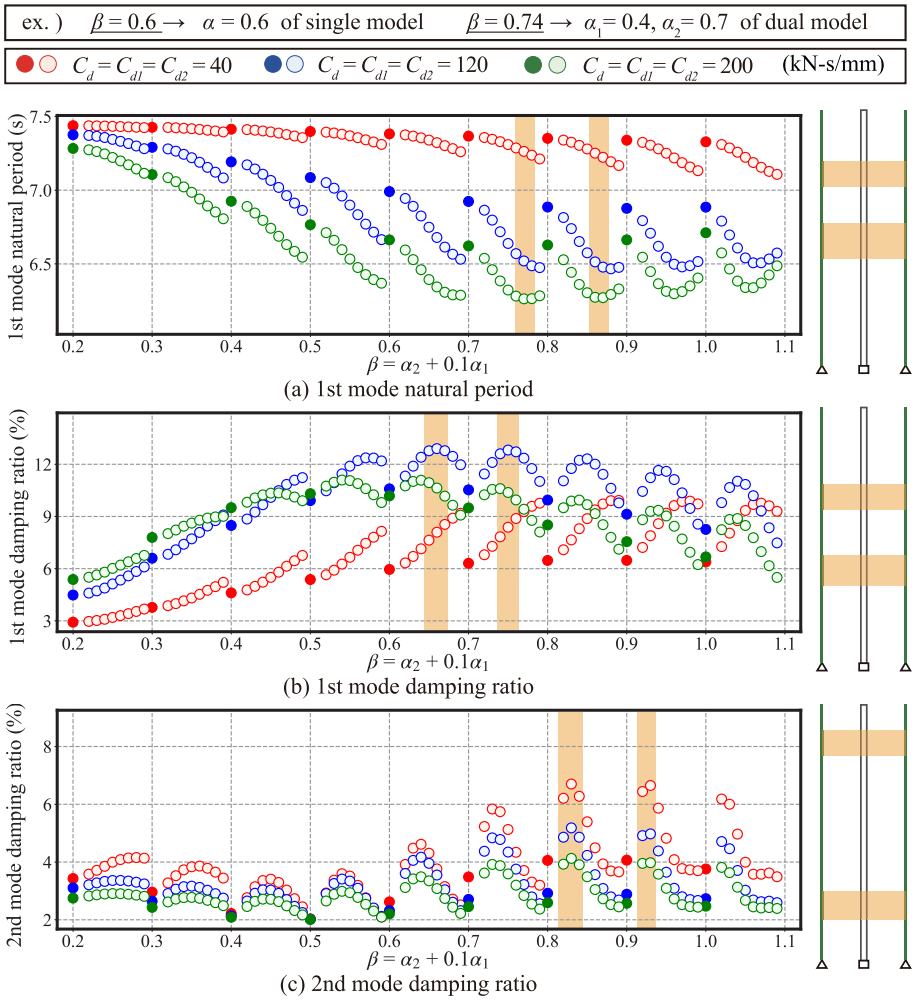

Fig. 11. Relationship between first and second mode characteristics and α_1, α_2, C_{d1}, C_{d2} ($k_{t1} = k_{t2} = 0.5 \times 10^6$ kN/m, 64-story).

The first and second mode shapes of the optimal model obtained by optimising the first mode characteristics ($\alpha_2 = 0.7$, $\alpha_1 = 0.6$) and the second mode characteristics ($\alpha_2 = 0.9$, $\alpha_1 = 0.25$) are shown in Fig. 12. As shown in Fig. 12, the optimal α_1 and α_2 correspond to the heights at which the rotation angle of the core is large enough to secure the perimeter column axial in each mode.

4.2. Optimal damping coefficient for first and second mode damping ratio

In this section, the optimal damping coefficient maximizing the first and second damping ratio is investigated. The contour maps (the x and the y axis correspond to the damping coefficient and the z-axis represents the first and second mode damping ratio) are shown in Figs. 13 and 14. Three models: model-2 which has an outrigger height ratio corresponding to the optimal outrigger height ratio maximizing the first mode damping ratio obtained in Section 4.1 ($\alpha_2 = 0.7$ and $\alpha_1 = 0.5$), model-1 without outriggers on the upper half of the building ($\alpha_2 = 0.5$ and $\alpha_1 = 0.5$,), and model-3 which is the truss model with the upper outrigger located at the top of the building ($\alpha_2 = 1.0$ and $\alpha_1 = 0.5$,) were considered.

First, the first mode damping ratio is maximized. As shown in Fig. 13 (a2) and Fig. 13(b2), the optimal damping coefficient in model2 is $C_{d2} =$ 40 kN-s/mm, $C_{d1} = 60$ kN-s/mm for 32-story model and $C_{d2} = 150$ kN-s/mm, $C_{d1} = 210$ kN-s/mm for 96-story model. Optimal C_{d1}, C_{d2} are proportional to the building height. The optimal C_{d1} value is larger than the optimal C_{d2} value because k_c/α is larger at the lower outrigger. As shown in Fig. 13(a1) and Fig. 13(b1), the optimal damping coefficient of model1 is larger than that of model2, because k_c/α is larger in model1. Similarly, as shown in Fig. 13(a3) and Fig. 13(b3), the optimal damping coefficient of model3 is smaller than that of model1 and model2. The optimal damper-connection stiffness ratios in model2 is $R_{db2} = 0.4$, $R_{db1} = 0.4$ for 32-story model and $R_{db2} = 0.6$, $R_{db1} = 0.55$ for 96-story model, where R_{db2} and R_{db1} are similar. The optimal damper-connection stiffness ratios in model1,3 are different from those for model2, indicating that the optimal damper-connection stiffness ratio varies with the outrigger height.

Next, second mode damping ratio is maximized. As shown in Fig. 14 (a2) and Fig. 14(b2), the optimum damping coefficient in model2 is about $C_{d2} = 20$ kN-s/mm and $C_{d1} = 40$ kN-s/mm for 32-story model and $C_{d2} = 60$ kN-s/mm and $C_{d1} = 120$ kN-s/mm for 96-story model. As the natural circular frequency (ω) in $k_d = C_d\,\omega$ is larger in higher modes, the optimal C_{d1} and C_{d2} values are smaller than those obtained by maximizing the first mode damping ratio. The optimal damper-connection stiffness ratio is also therefore smaller than that obtained by maximizing the first mode damping ratio. R_{db1} and R_{db2} were found to be in the range of 0.2–0.3 for all outrigger height ratios.

The contour plots obtained by maximizing the first and second mode damping ratio for $k_{t1} = k_{t2} = 1.0$ kN/m are shown in Fig. 15. The 96-story model2 is chosen as an example. As shown in Fig. 15, the larger the k_{t1} and the k_{t2}, the higher the first and second mode damping ratio, and so it is desirable to design the outrigger stiffness as large as possible in the dual outrigger system. Furthermore, the larger the k_{t1} and the k_{t2}, the larger the optimal damping coefficient, and the smaller the optimal damper-connection stiffness ratio.

From the above plots, it may be concluded that the optimal damping coefficient varies greatly depending on the building height, outrigger height ratio, outrigger stiffness, and kinds of seismic response. However, if an optimal design is not so important, an acceptable solution may be obtained with R_{db1} and R_{db2} in the range of 0.3–0.7.

4.3. Dominant mode in each seismic response

${}_iMDR_s$ (Mode Distribution of Response) shown in Eq. (4) and DR_s (Dominant Ratio) are defined in Eq. (5) to identify the dominant mode in each seismic response, where ${}_iA_s$ is the maximum response of the sth mode at ith node of the core, and n is the number of polymerized modes ($n = 6$ in this study). As shown in the equations, ${}_iMDR_s$ represents the contribution of each mode to the total CQC response, and by definition, the sum of the first ~n-th ${}_iMDR_s$ is then equal to the CQC response. DR_s represents the contribution of individual modal response to the maximum value at the ith node such that the sum of DR_s of first to nth mode is 100%.

$$ {}_iMDR_s = \frac{{}_iA_s^2}{\sum_{s=1}^{n} {}_iA_s^2} \times {}_iCQC\ ,\ \sum_{s=1}^{n} {}_iMDRs = {}_iCQC. \tag{4} $$

$$ DR_s(\%) = \frac{absmax({}_iA_s)^2}{\sum_{s=1}^{n=6} absmax({}_iA_s)^2} \times 100,\ \sum_{s=1}^{n=6} DR_s = 100. \tag{5} $$

${}_iMDR_s$ and DR_s of each seismic response are shown in Fig. 16. As shown in (a), the lateral displacement is dominated by first mode at all heights with $DR_1 \geq 98\%$. As shown in (b), although the contribution of the second mode is observed except in the middle layer which is the belly of second mode vibration, the story drift ratio is dominated by first mode with $DR_1 = 80\%$ and $DR_2 = 20\%$. As shown in (c), the second and third modes show significant contributions at all heights for lateral acceleration, with $DR_2 = 45\%$ and $DR_3 = 35\%$. As shown in (d), the overturning moment, which is more critical than the shear force to the whole system's collapse, is dominated by the first and second modes with $DR_1 = 35\%$ and $DR_2 = 41\%$.

${}_iMDR_s$ and DR_s of the optimal model maximizing the second mode damping ratio ($\alpha_2 = 1.0$ $\alpha_1 = 0.3$, $C_{d1} = C_{d2} = 40$ kN-s/mm) are shown in Fig. 17. The story drift ratio and lateral acceleration are shown as an example. Compared with Fig. 16, the first mode response is larger while the second mode response is smaller, resulting in a larger story drift ratio and a smaller acceleration. Therefore, by maximizing the second mode damping ratio, the second mode can be effectively controlled and the acceleration response can be reduced, but the displacement response may be large.

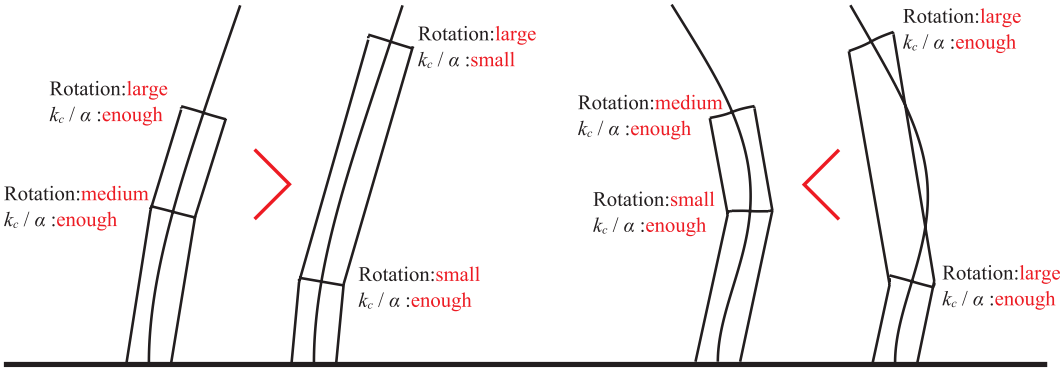

Fig. 12. Comparison of mode shapes ($\alpha_2 = 0.7$, $\alpha_1 = 0.6$ and $\alpha_2 = 0.9$, $\alpha_1 = 0.25$, 64-story).

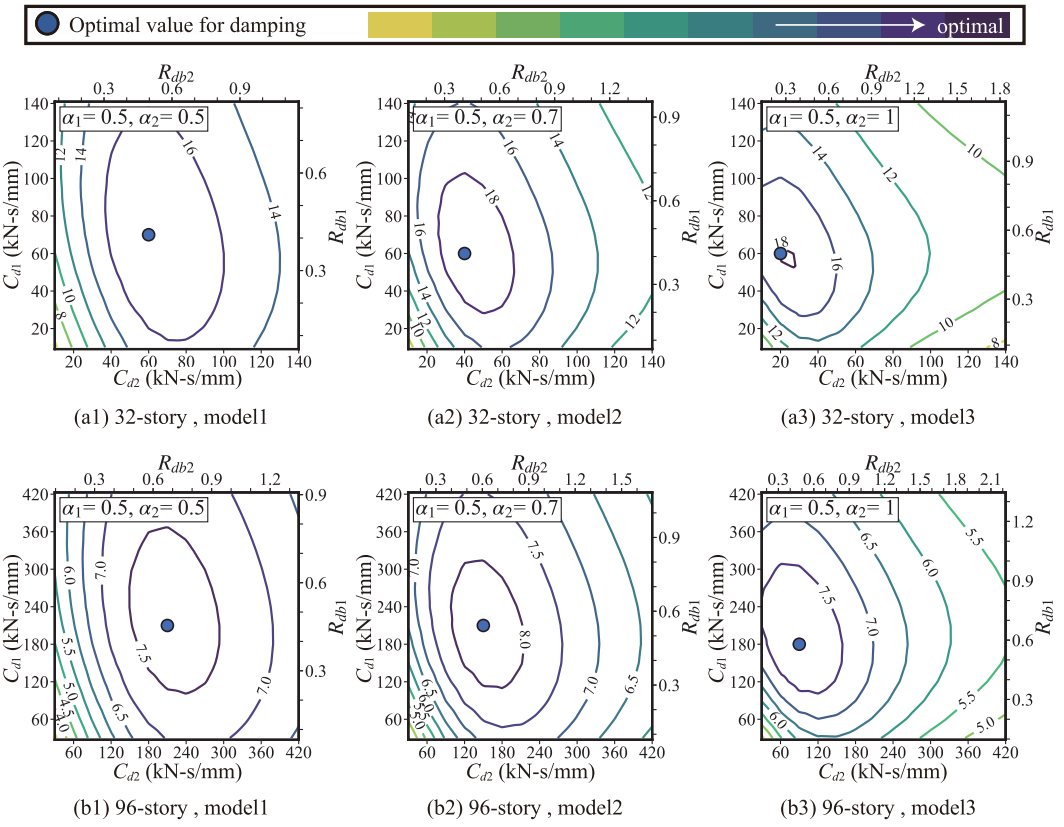

Fig. 13. Contour plots based on the first mode damping ratio ($k_{t1} = k_{t2} = 0.5 \times 10^6$ kN/m).

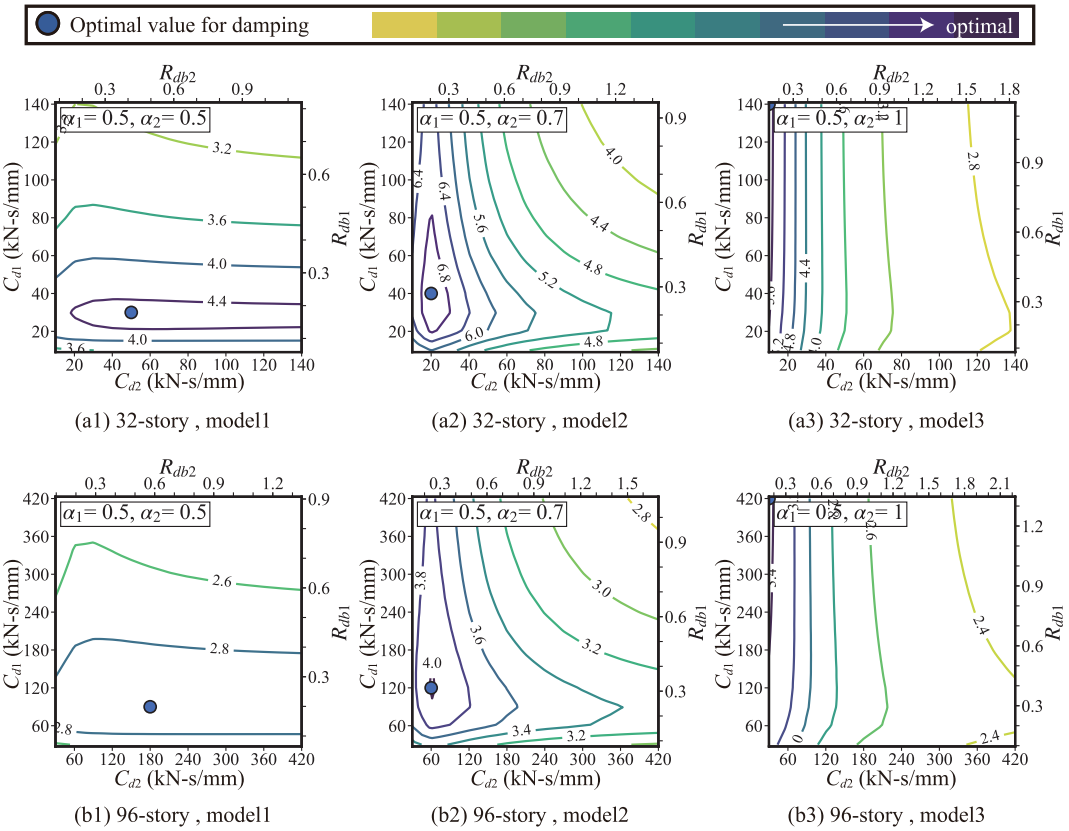

Fig. 14. Contour plot based on the second mode damping ratio ($k_{t1} = k_{t2} = 0.5 \times 10^6$ kN/m).

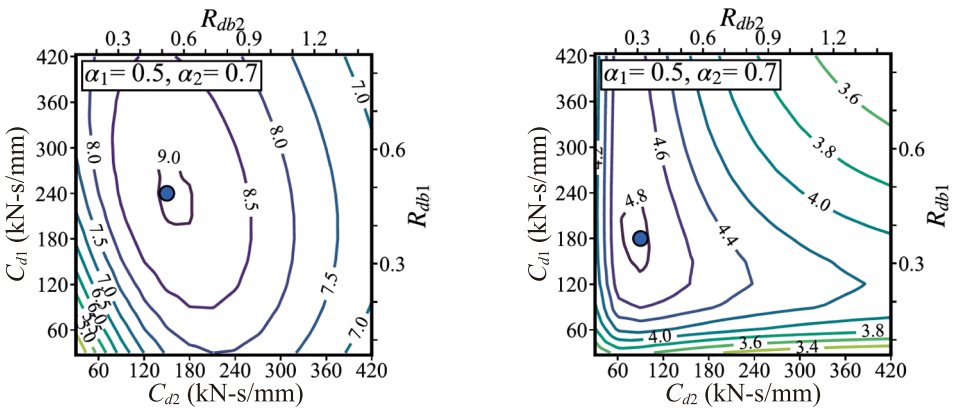

Fig. 15. Contour plots based on each modal damping ratio ($k_{t1} = k_{t2} = 1.0 \times 10^6$ kN/m, 96-story, model2).

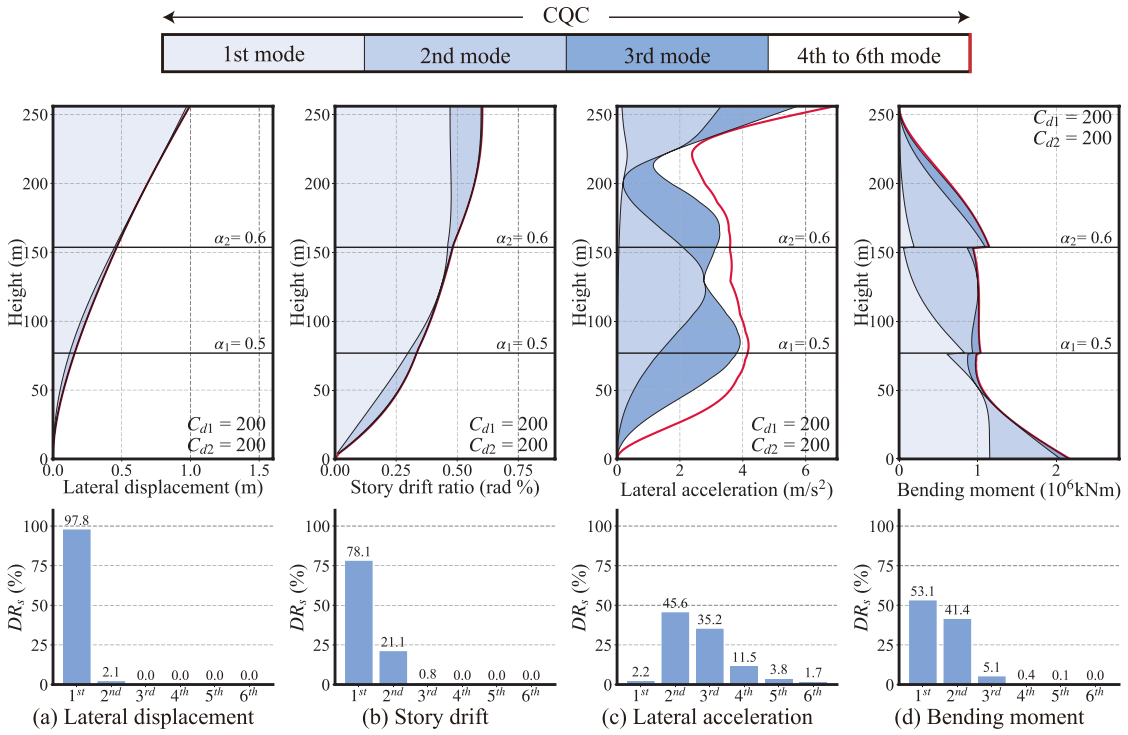

Fig. 16. Modal contributions to seismic response (top) and dominant ratios (bottom) ($k_{t1} = k_{t2} = 0.5 \times 10^6$ kN/m, 64-Story, $\alpha_2 = 0.7$, $\alpha_1 = 0.5$, $C_{d1} = C_{d2} = 200$ kN-s/mm).

4.4. Parametric study and optimal outrigger height ratio for seismic response

In this section, the optimal outrigger height ratio minimizing the seismic response is investigated and compared with the results discussed in Section 4.1. The relationships between α and each of the response parameters (the displacement, the acceleration, and the overturning moment) are shown in Fig. 18. As shown in Fig. 18, adding a lower outrigger to the single damped outrigger reduces each of the seismic response values. However, when the damping coefficient is large ($C_{d1} = C_{d2} = 200$ kN-s/mm) and the outrigger spacing is close ($\alpha_1 \geq 0.7$), the seismic response becomes larger than that in a single damped outrigger case. The optimal outrigger height ratios minimizing the roof displacement are $\alpha_2 = 0.7$–0.8 and $\alpha_1 = 0.6$–0.7, which are close to the corresponding optimal α values minimizing the first mode natural period and maximizing the first mode damping ratio. The optimal outrigger height ratios minimizing the roof acceleration are $\alpha_2 = 0.9$–1.0, and $\alpha_1 = 0.3$–0.4, which are close to the optimal α values corresponding to the maximum second mode damping ratio. These results indicate that optimal outrigger height ratios obtained based on minimizing the seismic response are highly dependent on dominant mode characteristics. The optimal outrigger height ratios corresponding to the minimum overturning moment are $\alpha_2 = 0.7$–0.8 and $\alpha_1 = 0.4$–0.5, which are therefore close to the optimal values based on the dominant first and second mode characteristics. These results are also comparable to those obtained in the previous study [13], and this suggests that the optimal outrigger height ratios are not significantly influenced by the choice of damper (viscous damper or elastoplastic dampers like the BRB). In summary, the ranges for optimal outrigger height ratios for dual damped outrigger are $\alpha_2 = 0.6$–1.0 and $\alpha_1 = 0.3$–0.7.

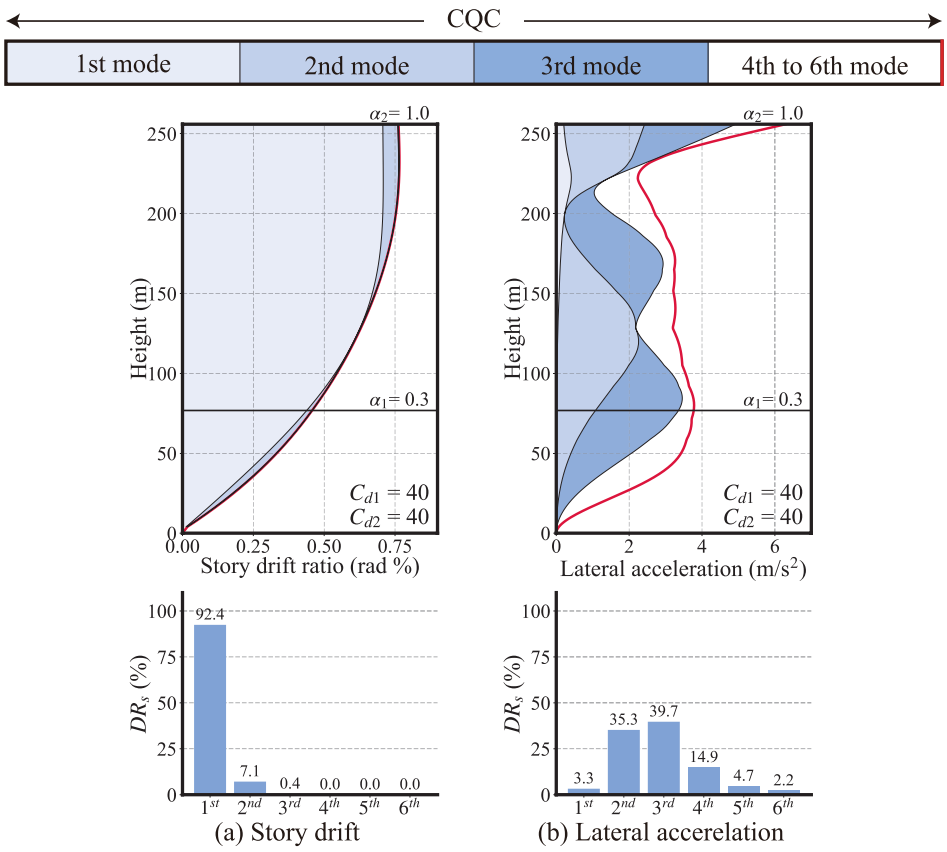

Fig. 17. Modal contributions to seismic response (top) and dominant ratios (bottom) ($k_{t1} = k_{t2} = 0.5 \times 10^6$ kN/m, 64-Story, $\alpha_2 = 1.0$, $\alpha_1 = 0.3$, $C_{d1} = C_{d2} = 40$ kN-s/mm).

4.5. Optimal damping coefficient for seismic response

The contour maps (the *x*- and the *y*-axis correspond to the damping coefficient and the *z*-axis represents the reduction ratio) for the roof displacement, the roof acceleration, and the overturning moment are shown in Fig. 19. The optimal values obtained based on the first and second mode characteristics are also plotted, and the results for model2 are shown as an example. As shown in Fig. 19(a1) and Fig. 19(a2), the optimum damping coefficient corresponding to minimum roof displacement is about $C_{d2} = 80$ kN-s/mm for 16-story model, $C_{d1} = 100$ kN-s/mm for 32-story model and $C_{d2} = 180$ kN-s/mm, $C_{d1} = 240$ kN-s/mm for 96-story model. As with the first mode damping ratio, the optimal damping coefficient increases with building height and optimal C_{d1} is larger than the optimal C_{d2}. The optimal damping coefficients corresponding to minimum roof displacement lie between the optimal values based on the first mode natural period (red △) and the first mode damping ratio (red x), which is due to the dominance of the first mode for the roof displacement. Similarly, as shown in Fig. 19(b1) and Fig. 19 (b2), the roof acceleration which is dominated by the higher modes, shows very small optimal damper characteristics as well as the second mode damping ratio (green x). As shown in Fig. 19(c1) and Fig. 19(c2), the optimal damping coefficients minimizing the overturning moment which is dominated by the first and second mode lie between the optimal amounts based on the first and second mode natural period and the damping ratios. Therefore, the distribution for each of the seismic response parameters are functions of the dominant modes of that response parameter explaining the difference in the corresponding optimal damping coefficients. However, the difference in the reduction ratio between the optimal value for each seismic response parameter (blue ●) and the optimal value based on maximizing the first mode damping ratio (red x) is less than 5%, indicating that each of the response parameters can be efficiently reduced by simply maximizing the first mode damping ratio.

The response reduction ratio of minimized seismic responses and the reduction ratios when (b) first mode damping ratio is maximized, (c) second mode damping ratio is maximized, and (d) first mode natural period is minimized, are shown in Table 3. As shown in Table 3(d), the roof acceleration and base shear may not be significantly reduced by minimizing the first mode natural period. Similarly, as shown in Table 3 (c), maximizing the second mode damping ratio may not be very efficient in reducing the roof displacement, the story drift ratio and the overturning moment. However, as shown in Table 3(b), maximizing the first mode damping ratio reduced the displacement response and acceleration response significantly. This indicates the effectiveness of maximizing the first mode damping ratio for spectrally matched waves.

4.6. Seismic response against Japanese long period earthquake (KA1)

In this section, the seismic response from the input KA1 wave is compared with the responses obtained from the spectrally matched waves. First, ${}_i MDR_s$ and DR_s for the Story drift ratio, the roof acceleration, and the overturning moment are shown in Fig. 20. If compared with the response from the spectrally matched waves, the dominance of higher modes is small because the spectral values corresponding to the second and third periods are smaller for the KA1 wave as shown in Fig. 7.

Fig. 21 shows the contour plot where the *z*-axis represents the reduction ratio of the story drift ratio and roof acceleration obtained from the KA1 wave. The *xy*-axis in Fig. 21(a1) and Fig. 21 (a2) represent the outrigger height ratio, and the *xy*-axis in Fig. 21(b1) and Fig. 21(b2) represent the damping coefficient. As shown in Fig. 21(a1), the optimal α_2 and α_1 minimizing the story drift ratio is closer to the optimal α_2 and α_1 values based on the first mode characteristics than those obtained by

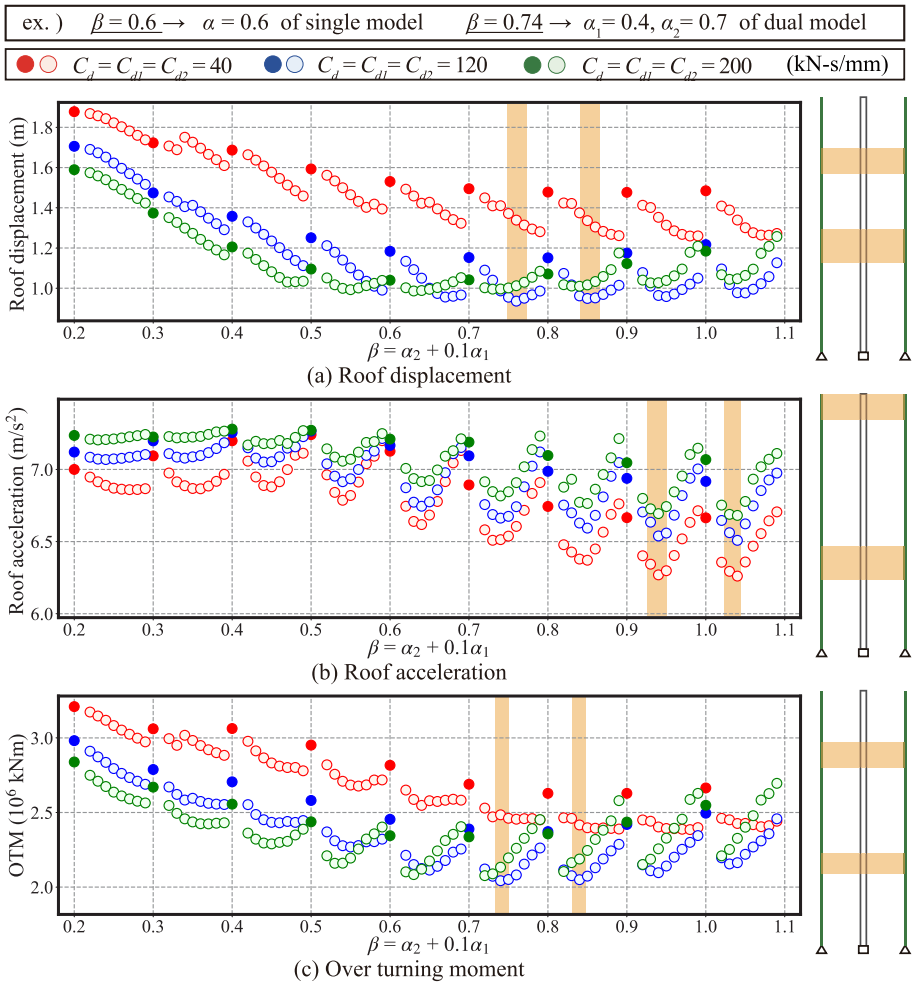

Fig. 18. Relationship between seismic response and α_1, α_2, C_{d1}, C_{d2} ($k_{t1} = k_{t2} = 0.5 \times 10^6$ kN/m, 64-Story).

minimizing the story drift from the spectrally matched waves. This might be because DR_2 is lower for the KA1 wave. As shown in Fig. 21 (a2), the optimal α_2 and α_1 based on the roof acceleration are closer to the second mode characteristics than the corresponding values obtained from the spectrally matched waves, because of lower DR_3. As shown in Fig. 21(b1), the optimal damping coefficients minimizing the response from KA1 wave are larger than those based on the responses from spectrally matched waves. This might be because the displacement response spectra of the KA1 wave is steeper in the period range of 6.2–6.5 s, and so the effect of the shorter period is larger. Similarly, the optimal damping coefficients minimizing the roof acceleration (Fig. 21 (b2)) are greater than those based on the responses from spectrally matched waves. Furthermore, the difference in the reduction ratio between the optimal value for each seismic response parameter (labelled with blue marker ●) and the optimal value based on maximizing the first mode damping ratio (labelled with red marker x) is less than 5%, indicating that even though the optimal damping coefficients depend on the input ground motion characteristics, maximizing the first mode damping is sufficient enough to efficiently reduce each of the responses.

4.7. Discussion

In Sections 4.1–4.6, it was shown that the dual damped outrigger system is effective in controlling not only the first mode but also the second mode response. While all the response parameters were significantly reduced by maximizing the first mode damping ratio, the displacement response could not be efficiently reduced by maximizing the second mode damping ratio. Therefore, considering the conclusions of Chapter 3 and Chapter 4, maximizing the first mode damping ratio is the best approach overall for the damped outrigger system.

Furthermore, the optimal outrigger height ratio is about $\alpha = 0.5$–0.8 for single damped outrigger, $\alpha_2 = 0.6$–1.0, $\alpha_1 = 0.3$–0.7 for dual damped outrigger, while the optimal damping coefficient vary greatly for each design variable (for example, the building height or the outrigger height). Furthermore, as mentioned in Chapter 1, while the outrigger height and stiffness of each member are generally predetermined during the planning stage, the damping coefficients have a relatively high degree of freedom in design. Therefore, it is necessary to develop an optimal design method that accommodates these constraints and allows for changes in the design variables.

5. First mode characteristics of triple, quad damped outrigger

In this section, the number of outriggers is further increased to three or four, and the extent to which the first mode characteristics are improved is investigated. Analysis models with triple and quad damped outriggers are listed in Table 4. As shown in Table 4, triple and quad damped outrigger systems have a large number of design variables, and so models with unrealistic parameters (for example, a model where the uppermost outrigger is located at the bottom of the building) are excluded from the analysis range. The relationship between the first mode characteristics and the outrigger height ratio is shown in Fig. 22. 64-story models with $k_{t1} = k_{t2} = k_{t3} = k_{t4} = 0.5 \times 10^6$ kN/m, and $C_{d1} = C_{d2} = C_{d3} = C_{d4} = 120$ kN-s/mm are considered. As shown in Fig. 22, the

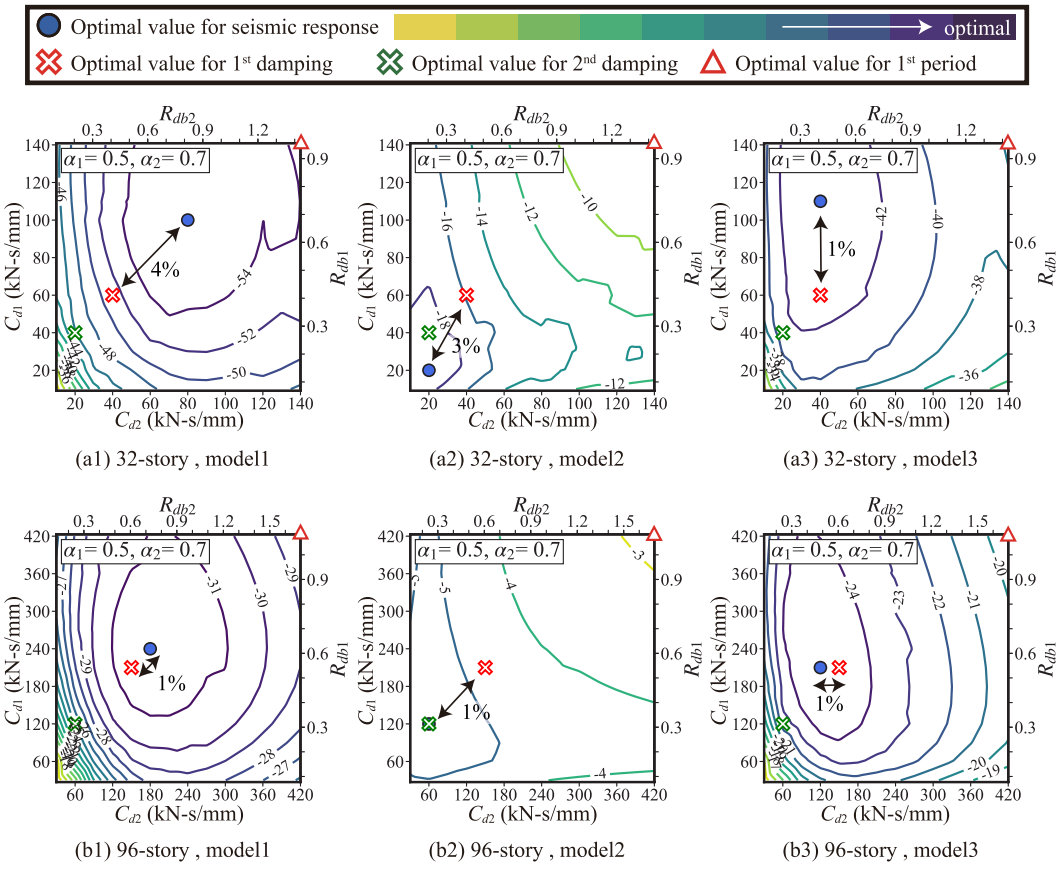

Fig. 19. Contour plots of seismic response reduction ratio ($k_{t1} = k_{t2} = 0.5 \times 10^6$ kN/m, model2).

Table 3
Summary of seismic response reduction ratios ($k_{t1} = k_{t2} = 0.5 \times 10^6$ kN/m).

	Story	(a) Minimized seismic response	(b) Maximized first mode damping ratio		(c) Maximized second mode damping ratio		(d) Minimized first mode natural period	
		Reduction ratio (%)	Reduction ratio (%)	Error from (a)	Reduction ratio (%)	Error from (a)	Reduction ratio (%)	Error from (a)
Roof displacement (RD)	16	82.4	75.1	-7.27	56.0	-26.41	69.2	-13.18
	32	55.8	51.5	-4.29	32.2	-23.58	53.0	-2.77
	64	53.4	50.4	-3.02	31.0	-22.47	44.4	-9.02
	96	31.8	31.7	-0.17	17.9	-13.88	26.7	-5.15
Story drift ratio (SD)	16	83.8	75.5	-8.34	56.2	-27.63	70.6	-13.26
	32	56.6	50.2	-6.41	33.1	-23.49	51.1	-5.49
	64	52.4	47.8	-4.57	31.8	-20.57	42.3	-10.15
	96	31.8	29.9	-1.83	18.9	-12.83	25.2	-6.62
Roof acceleration (RA)	16	41.0	29.9	-11.01	38.0	-2.96	16.3	-24.64
	32	26.2	14.9	-11.34	23.3	-2.91	5.6	-20.64
	64	15.2	9.4	-5.80	12.9	-2.37	3.6	-11.61
	96	7.9	3.9	-4.01	7.1	-0.76	0.8	-7.04
Base shear (BS)	16	54.0	42.2	-11.85	51.0	-3.03	13.4	-40.66
	32	34.3	24.5	-9.77	30.7	-3.51	10.7	-23.53
	64	25.9	20.4	-5.49	25.2	-0.74	10.2	-15.74
	96	16.5	10.9	-5.62	15.6	-0.87	4.6	-11.93
Over turning moment (OTM)	16	74.8	66.2	-8.61	55.5	-19.29	50.3	-24.52
	32	46.4	41.0	-5.42	33.3	-13.09	34.6	-11.85
	64	42.3	39.6	-2.68	30.9	-11.36	28.9	-13.36
	96	25.6	23.5	-2.05	19.1	-6.44	15.8	-9.74

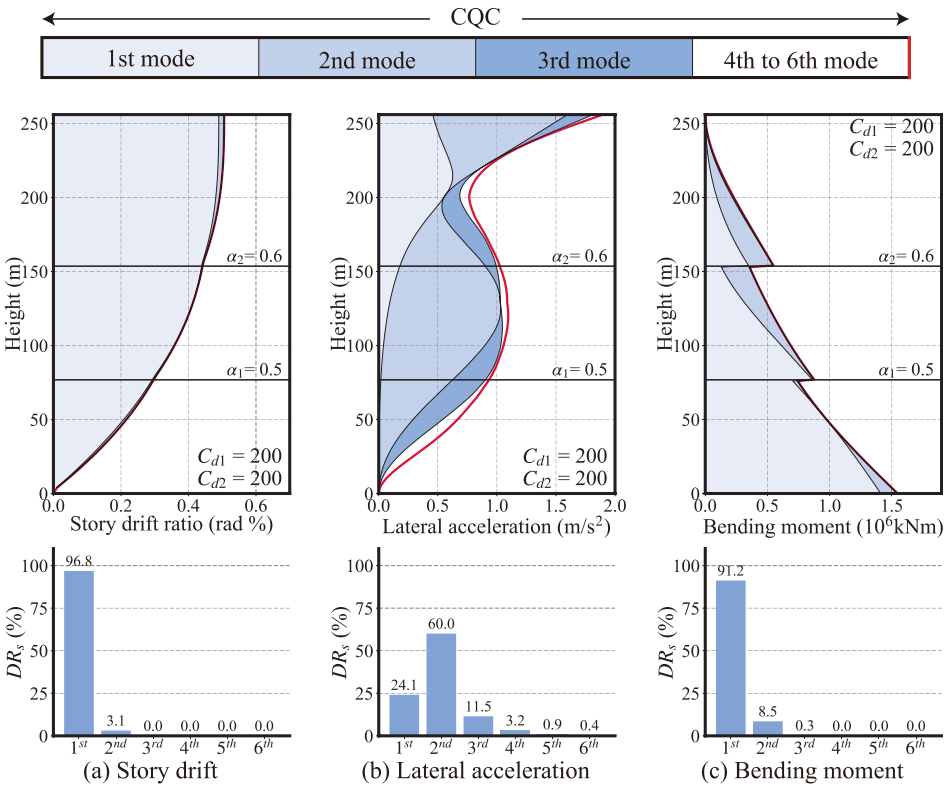

Fig. 20. Modal contributions to seismic response (top) and dominant ratios (bottom) against KA1 wave ($k_{t1} = k_{t2} = 0.5 \times 10^6$ kN/m, 64-Story).

first mode natural period is 6.66 s, 6.29 s, 6.17 s, and 6.13 s for the single, dual, triple, and quad outrigger system, respectively and the first mode damping ratio is 10.6%, 12.9%, 13.5%, and 13.6% for the single, dual, triple, and quad outrigger, respectively. As was seen when adding outriggers to a single outrigger, the period reduces and the damping ratio increases when the number of outriggers is increased, but the rate of increase decreases. Thus, the effect of outrigger addition diminishes and the first mode natural period and the first mode damping ratio converge to about 6.1 s and 14%, respectively.

6. Proposal of a generalized optimal design procedure for damped outrigger systems with additional linear viscous dampers

According to the analysis results in Sections 3 and 4, it may be inferred that the requirements (IV) and (V) mentioned in the introduction may be satisfied by adopting a design guideline that maximizes the first mode damping ratio. For this purpose, it is necessary to formulate simple design equations to estimate the damper coefficient maximizing the first mode damping ratio. Nevertheless, this optimized damper coefficient is an idealized (sometimes unrealistic) target value used in the preliminary design stage, and, in the actual design process, is required to be adjusted considering the practicalities (e.g., the capacity limitation of the damper device, the construction cost, or the engineer's intention.) as per the requirements (I), (II), and (III). Therefore, it is also necessary to develop a design tool checking the first mode characteristic of arbitrary linear damped outrigger systems in this iterative design process. In Section 6.1, an equation to estimate the damper-connection stiffness ratio that maximizes the first mode damping ratio under the constraints of the outrigger height ratio and the connection-core stiffness ratio will be developed. In Section 6.2, a machine learning model that predicts the first mode characteristics will be developed. In Sections 6.3 and 6.4, a web-based design tool that incorporates the estimation equation and the machine learning model will be developed and the way to use the design tool is demonstrated through a design example of single- to quad-damped outrigger systems. In Section 6.5, a generalized optimal design procedure for damped outrigger systems with additional linear viscous dampers based on the entire study is proposed.

6.1. Optimal damping coefficient based design equation

Design equations (6) to (9) for single to quad damped outrigger are proposed to approximately estimate the optimal damper to connection stiffness ratio (R_{dbi}) based on complex eigenvalue analysis. These equations estimate the optimal damper-connection stiffness ratio that maximizes the first damping ratio in the specified range of the outrigger height ratio (α_i) and connection to core stiffness ratio (S_{bci}), allowing for flexibility in the outrigger height and stiffness of each element. The calibration coefficients of these equations are listed in Table 5.

$$R_{db} = C1 \times \alpha^{C2} \times S_{bc}^{C3} + C4. \tag{6}$$

$$R_{db1,2} = C1 \times \alpha_1^{C2} \times \alpha_2^{C3} \times S_{bc1}^{C4} \times S_{bc2}^{C5} + C6. \tag{7}$$

$$R_{db1,2,3} = C1 \times \alpha_1^{C2} \times \alpha_2^{C3} \times \alpha_3^{C4} \times S_{bc1}^{C5} \times S_{bc3}^{C6} \times S_{bc3}^{C7} + C8. \tag{8}$$

$$R_{db1,2,3,4} = C1 \times \alpha_1^{C2} \times \alpha_2^{C3} \times \alpha_3^{C4} \times \alpha_4^{C5} \times S_{bc1}^{C6} \times S_{bc2}^{C7} \times S_{bc3}^{C8} \times S_{bc4}^{C9} + C10. \tag{9}$$

For example, a dual damped outrigger (Eq. (7)) is considered. Fig. 23 shows the plots of the optimal damping coefficients (C_{d1}, C_{d2}, R_{db1}, R_{db2}) and β. As shown in the Fig. 23, Eq. (7) accurately captures the trend of these optimal damping coefficients. The first mode natural period, the first mode damping ratio, the second mode damping ratio, the story drift ratio, and the roof acceleration obtained using Eq. (7) are shown in Fig. 24. The first mode natural period from Eq. (7) is approximately the average of all the optimal results. As shown in Fig. 24 (b), the first mode damping ratio obtained from Eq. (7) is the maximum of all the obtained results. As shown in Fig. 24 (c), the second mode damping ratio obtained from Eq. (7) lies at about two-third of the maximum of the total analysis

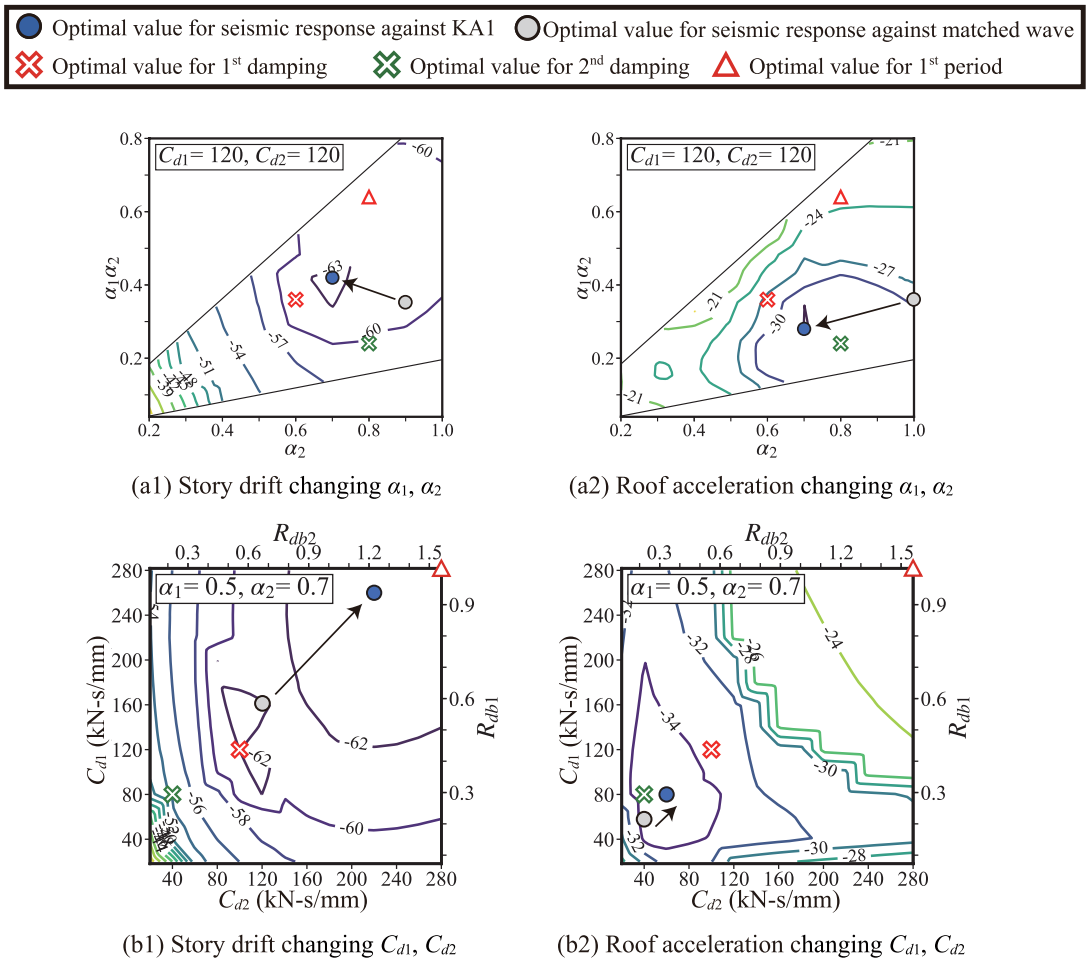

Fig. 21. Contour plots of seismic response reduction ratio against KA1 ($k_{t1} = k_{t2} = 0.5 \times 10^6$ kN/m, 64-Story, model2).

Table 4
Analysis range of triple and quad models.

	triple model	quad model
Story	32, 64, 96	64, 96
k_{t1}–k_{t4}	0.25, 0.5, 1.0	0.25, 0.5, 1.0
α_1	0.3–0.7 @ 0.1	0.3–0.7 @ 0.1
α_2	0.3–0.7 @ 0.1	0.3–0.7 @ 0.1
α_3	0.5–1.0 @ 0.1	0.3–0.7 @ 0.1
α_4		0.6–1.0 @ 0.1
C_{d1}–C_{d4}	10–140 @ 10 (32)	
	20–280 @ 20 (64)	20–280 @ 20 (64)
	30–420 @ 30 (96)	30–420 @ 30 (96)
total model	3,704,400	144,060,000

results. As shown in Fig. 24 (d), the story drift ratio obtained from Eq. (7) is low, but because the estimated first mode natural period average of all results, some models have drifts lower than that of the model estimated using Eq. (7). As shown in Fig. 24 (e), the reduction of the roof acceleration is also expected because additional damping in the second mode may be obtained by using a dual damped outrigger. In conclusion, by applying Eq. (7), the first mode damping ratio can be maximized, and both displacement response and acceleration response can be reduced greatly. The accuracy of the other equations (11), (13), and (14) were also similarly verified.

6.2. Machine learning model to estimate the first mode characteristics

A decision tree is an algorithm that classifies or regresses data by repeating Yes or No questions. An example of how a decision tree algorithm works is shown in Fig. 25.

Next, an example of how a gradient boosting algorithm works is shown in Fig. 26. The gradient boosting algorithm is performed as follows:

Randomly divide the input data into train_data, eval_data, and test_data.
Create the i-th decision tree (a learning model) using the train_data by a decision tree algorithm.
Predict the first mode damping ratio by the i-th decision tree, using both the train_data and the eval-data from.
Calculate the error from the predicted value and the correct answer value. In this proposal, R^2 score was used as the error indicator.
Create the $i + 1$-th decision tree to minimize a loss function calculated by the error.
Calculate the error prediction from the $i + 1$-th decision tree (⑤.)
Add the prediction value (③) and the error prediction value (⑥), and calculate the second prediction value considering the error.
Calculate the error again from the predicted value (⑦) and the correct answer value.
Converge ④ ~ ⑧ to the specified tolerance.
Finally, confirm the accuracy of the learining model using the train_data.

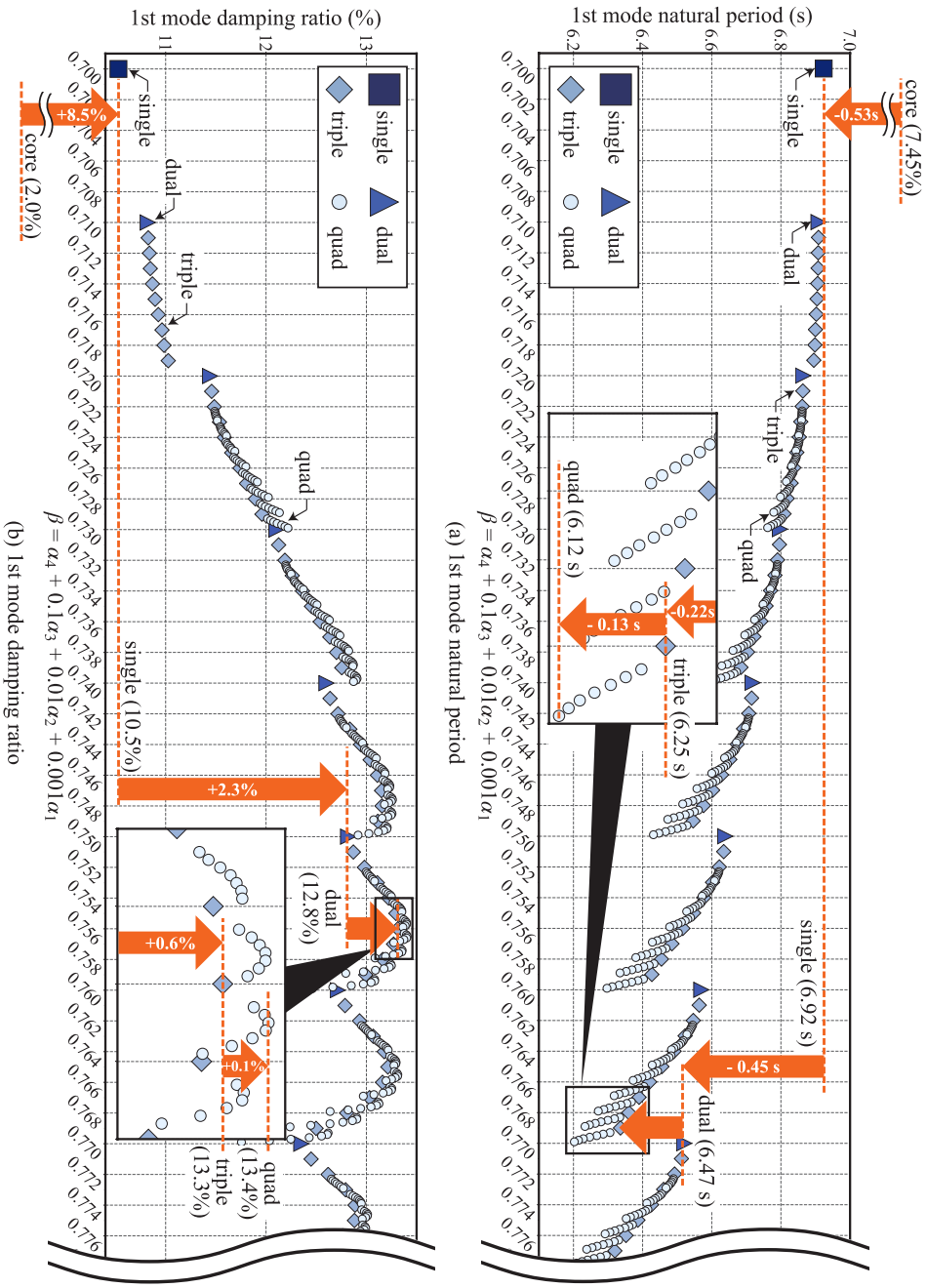

Fig. 22. first mode characteristics of triple and quad model (64-story, $k_{t1\sim4} = 0.5 \times 10^6$ kN/m).

Using the gradient boosting method described in Fig. 26, a machine learning model is proposed to estimate the first mode characteristics of the damped outrigger system. The explanatory variables are building height, $\alpha_{1\sim4}$, $S_{bc1\sim4}$, and $R_{db1\sim4}$, and the objective variables are the first mode natural period and the first mode damping ratio. The hyper-parameters are tuned using the Optuna library [26].

The change in score (degree of freedom adjusted coefficient of determination: R^2) in the convergence process (⑩) is shown in Fig. 27. The comparison between the predicted value and the test value is also shown in Fig. 28. A triple damped outrigger is shown as an example and the R^2 score is over 0.99 against eval_data, which confirms the high accuracy of the learning model. As shown in Fig. 28, the predictions for both the first mode natural period and the first mode damping ratio captures the correct answer value with less than 5% error.

6.3. Web application-based design tool

An optimal design kit composed of the design equations and the learning models is consolidated into a web application since it is difficult for engineers to use the proposed learning models directly. The instruction for use are as follows (Fig. 29):

(1) Access the page from the URL or the QR code,
(2) Select the number of outriggers (e.g., 3 layers),
(3) Enter the building height, $\alpha_{1\sim3}$, $S_{bc1\sim3}$, and $R_{db1\sim3}$, which activates the learning model for the first mode characteristics.

The output values are the first mode natural period and the first mode damping ratio. The optimal damper-connection stiffness ratio and the first mode characteristics by the proposed design equations

Table 5
Coefficient of the simple design equations.

(a) single model, Equation (6)

	C1	C2	C3	C4
R_{db}	−0.870	0.284	0.309	1.283

(b) dual model, Equation(7)

	C1	C2	C3	C4	C5	C6
R_{db1}	−1.043	0.158	0.011	0.265	−0.130	1.383
R_{db2}	−2.834	0.079	0.106	0.034	0.031	2.946

(c) triple model, Equation (8)

	C1	C2	C3	C4	C5	C6	C7	C8
R_{db1}	2.019	−0.044	−0.090	0.069	−0.059	−0.163	0.187	−1.655
R_{db2}	−1.129	0.132	0.238	−0.075	0.085	0.241	−0.217	1.344
R_{db3}	−1.514	0.107	0.276	0.387	0.186	−0.079	0.026	1.463

(d) quad model, Equation (9)

	C1	C2	C3	C4	C5	C6	C7	C8	C9	C10
R_{db1}	1.232	−0.048	−0.106	−0.123	0.106	−0.052	−0.172	−0.088	0.274	−0.920
R_{db2}	2.005	−0.030	−0.046	−0.097	0.067	−0.014	−0.049	−0.152	0.184	−1.726
R_{db3}	−0.990	0.062	0.164	0.273	−0.120	0.140	−0.106	0.301	−0.212	1.158
R_{db4}	−1.269	0.072	0.115	0.541	0.673	0.205	−0.034	0.082	−0.067	1.110

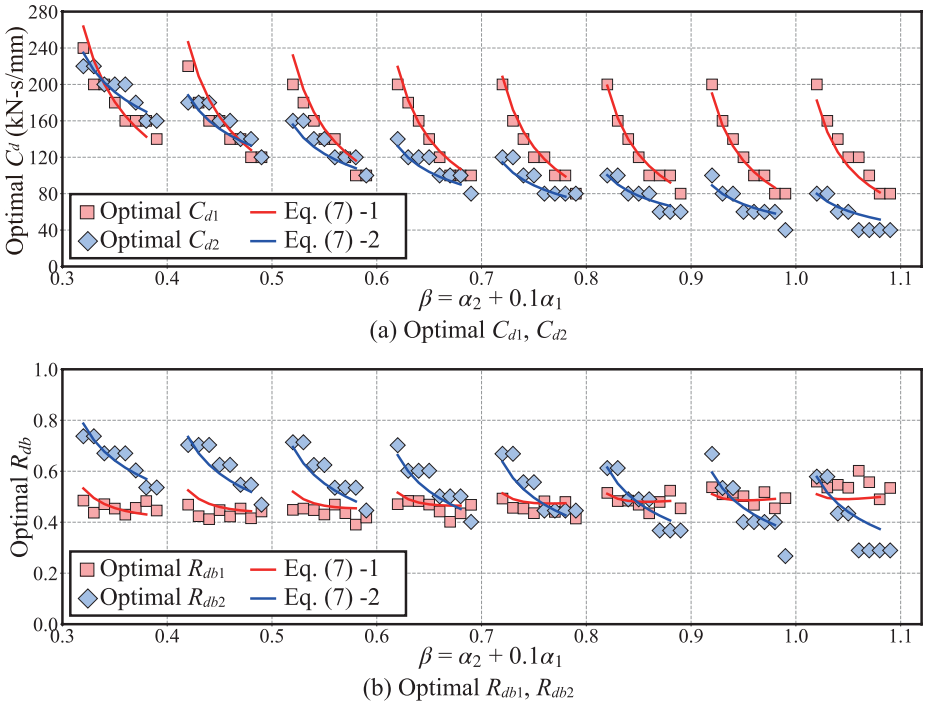

Fig. 23. Relationship between the optimal damping coefficients and β (64-Story).

considering the input $\alpha_{1\sim3}$, $S_{bc1\sim3}$ are also displayed.

A case study for design of a 64-story dual damped outrigger system where $k_{t1,2}$ is 0.5 × 10^6 kN/m, α_1 is 0.5, α_2 is 0.7, S_{bc1} is 0.7 and S_{bc2} is 0.5 is demonstrated. In this case, the optimal damping coefficients calculated from the design equations are C_{d1} = 110 kN-s/mm, C_{d2} = 61 kN-s/mm, and the first mode characteristics obtained from the machine learning tool are T_1 = 6.79 s and ξ_1 = 11%. If the damping coefficient is too large causing the budget to exceed, $k_{t1,2}$ can be reset to 0.2 × 10^6 kN/m and recalculating the explanatory variables, the damper may be redesigned using C_{d1} = 186 kN-s/mm, C_{d2} = 62 kN-s/mm, and T_1 = 6.86 s, ξ_1 = 10.31%. Similarly, performance can be improved by increasing, $k_{t1,2}$ to 0.8 × 10^6 kN/m and recalculating explanatory variables, the damper may be redesigned using C_{d1} = 138 kN-s/mm, C_{d2} = 82 kN-s/mm, and T_1 = 6.67 s, ξ_1 = 13%. In this way, optimal design satisfying the required damping coefficient (ensuring economic efficiency) and first-order mode characteristics (ensuring performance) can be obtained. The same procedure can also be used to accommodate other variations in architectural plans. It is also possible to select the number of outriggers by comparing the optimal models (single to quad damped outrigger systems), as discussed in Section 6.4.

6.4. Design example

This section outlines the application of the proposed optimal design kit using five different models. As shown in Fig. 30, four (single to quad) outrigger models with outriggers equally distributed along the height

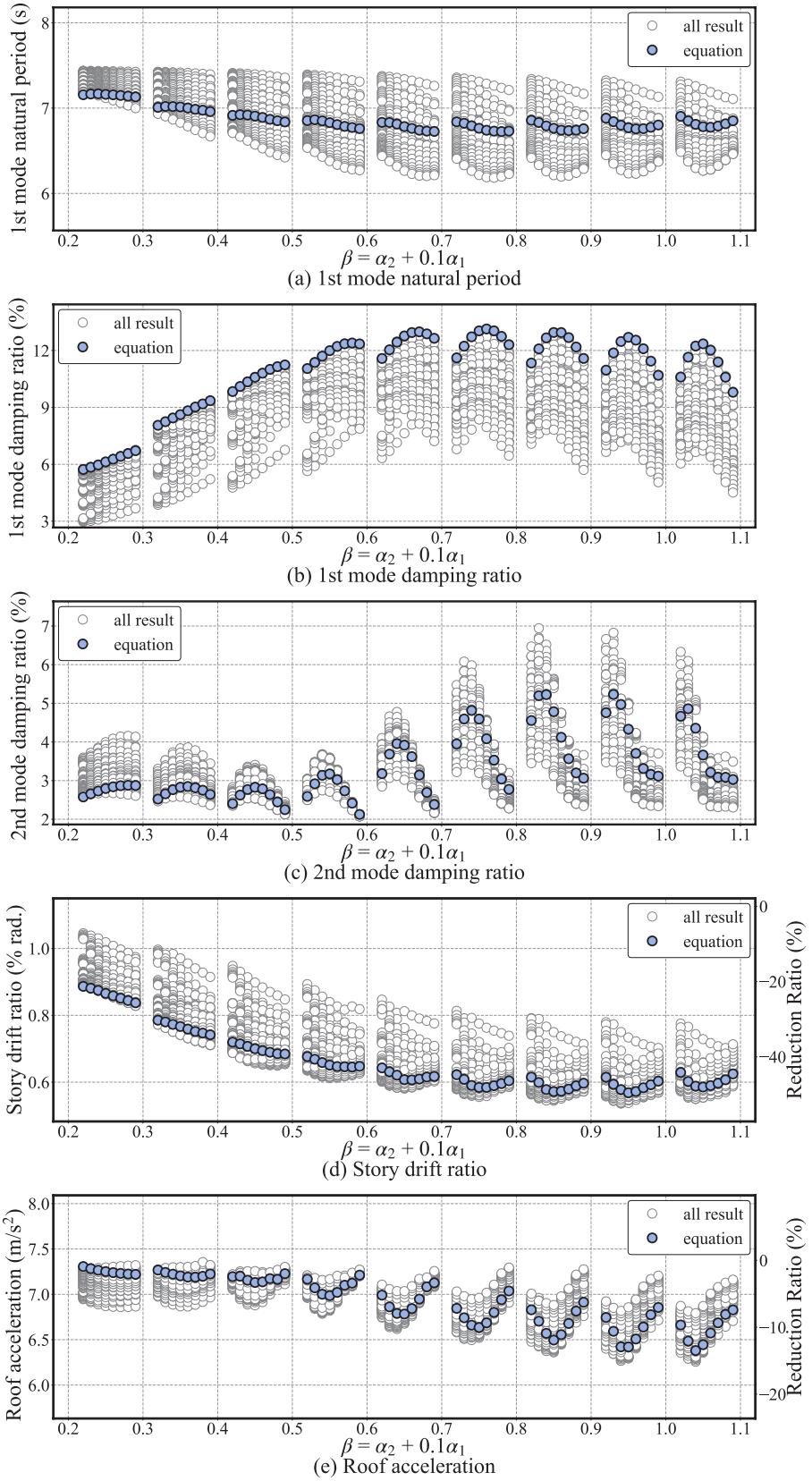

Fig. 24. Optimal models obtained from the proposed equation ($k_{t1,2} = 0.5 \times 10^6$ kN/m, 64-Story).

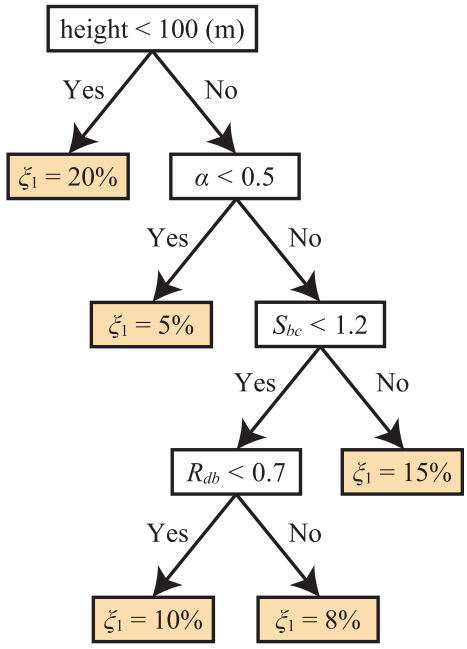

Fig. 25. Schematic diagram of decision tree algorithm.

are considered along with a bare core model. The building height is 256 m (64-story) and the outrigger stiffness k_{t1} ($=k_{t2} = k_{t3} = k_{t4}$) is taken as 0.5×10^6 kN/m. The optimal damping coefficients evaluated from the design equations are shown in Fig. 30. The acronyms RD, SD, RA, BS, and OTM in Fig. 30 correspond to the roof displacement, story drift ratio, roof acceleration, base shear, and overturning moment, respectively.

As shown in Fig. 30(b), the first mode damping ratio estimated by the machine learning model agrees well with the analytical values. While the first mode damping ratio increases as the number of outriggers increases, the rate of increase decreases after the second outrigger is included, which is consistent with the results of Chapter 5. On the other hand, the second and third mode damping ratios increase in proportion to the number of outriggers. This confirms that increasing the number of outriggers is more efficient in achieving higher modal damping ratios than optimizing the dampers individually.

As shown in Fig. 30(c), the roof displacement, story drift ratio and overturning moment, which are dominated by the first mode, are significantly reduced by adding the first damped outrigger (i.e., single damped outrigger), and the rate of response reduction decreases with subsequent additions. On the other hand, the roof acceleration and base shear are dominated by yet higher modes and so significant reduction is observed with each addition of the outrigger and the reduction is in proportion to the number of outriggers. Based on this result, it is proposed to optimally design a single damped outrigger based on the first mode characteristics when only the displacement response is to be

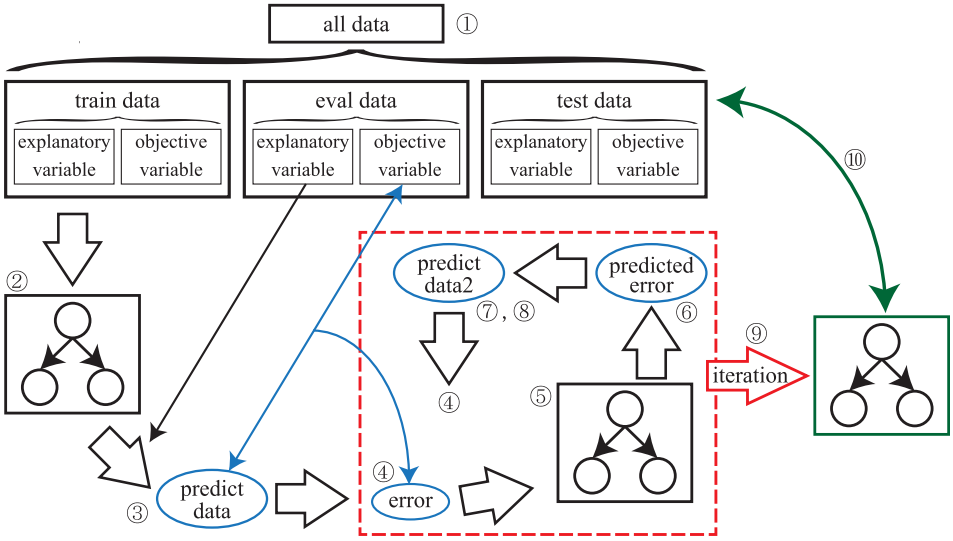

Fig. 26. Schematic diagram of gradient boosting algorithm.

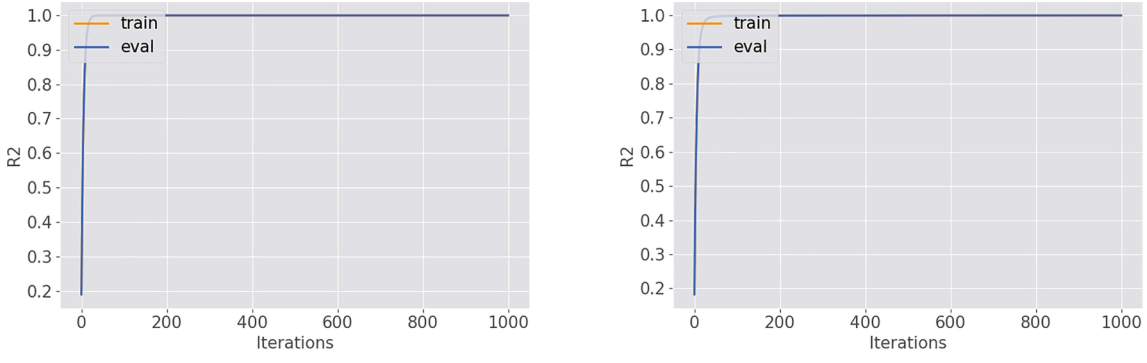

Fig. 27. R^2 score of machine leaning model (triple).

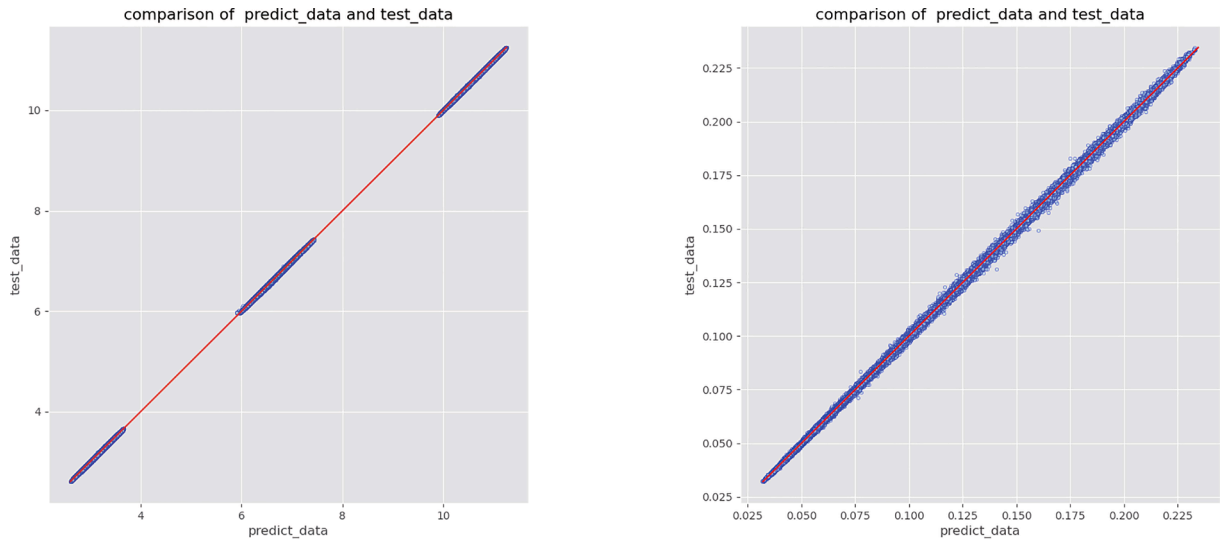

(a) 1st mode natural period (b) 1st mode damping ratio

Fig. 28. Comparison of predicted value and true value (triple).

reduced, and multiple damped outriggers should be considered when reduction in acceleration and base shear response is also desired.

6.5. Generalized design procedure

Based on the results of the present study, ranging from the numerical investigation to the development of the web application-based design tool and the actual design practice, a generalized optimal design procedure for damped outrigger systems with additional linear viscous dampers is proposed as follows:

Step 1. Determine the maximum available number of outriggers from the viewpoint of architectural, mechanical, electrical and plumbing planning. It is recommended to use all the available outriggers as damped outriggers to increase the higher mode damping ratios.
Step 2. Determine the appropriate outrigger heights based on the presented numerical results, and then design the damper coefficients to maximize the first mode damping ratio by using the proposed design equations. In the preliminary design stage, assume the outrigger stiffness k_t as 0.5×10^6 kN/m (i.e a standard value). Use the damper coefficient calculated from the design equations as the idealized target value in this stage. Note that the damper coefficient obtained iteratively in the next step is practically the true optimized value.
Step 3. Estimate the first mode characteristic by using the proposed web application-based design tool. If the designed damper coefficients are unrealistic because of the capacity limitation of the damper device or the construction cost, decrease the damper coefficients. If a shorter first mode natural period is expected, increase the damper coefficients. In either case, adjust the damper coefficients iteratively while checking the first mode characteristic. If a higher maximized first mode damping ratio or a much shorter first mode natural period is expected, design the stiffer outrigger truss or increase the number of the damped outriggers (the negotiation with the architectural designer is required.) Note that the larger the number of damped outriggers, the smaller the optimal damper coefficient of each damped outrigger.
Step 4. Perform LRHAs on the DM model to evaluate the seismic responses. If the demands (e.g., the story drifts, the floor accelerations, the member forces, etc.) are considerably lower than those permitted by the design criteria, the damper coefficients may be decreased.

7. Conclusion

The following conclusions were drawn from this study:

1) For a single damped outrigger system, the optimal outrigger height ratio minimizing the period, maximizing the damping ratios, and maximizing the seismic response reduction was found to range from 0.5 to 0.9. The optimal damping coefficient and damper-connection stiffness ratio were found to vary depending on the chosen seismic response parameter, but maximizing the first mode damping ratio was found to be the best aproach to reduce the displacement response.
2) For dual damped outrigger systems, the optimal outrigger height ratios α_2 and α_1 minimizing the period, maximizing the damping ratios, and maximizing the seismic response reduction were found to be in the ranges of 0.6–1.0 and 0.3–0.7 respectively. The optimal α_2 values are slightly larger than that of the single damped outrigger. Further, the optimal damping coefficient in the lower layer was found to be larger than that in the upper layer. The optimal damping coefficient and damper-connection stiffness ratio vary depending on the chosen seismic response parameter, but maximizing the first mode damping ratio was found to be the best aproach to effectively reduce both the displacement and acceleration response.
3) For optimal design, it was proposed to maximize the first mode damping ratio based on the response from single and dual damped outrigger systems. If the number of outriggers is increased to two or more, the second mode damping ratio can also be increased although this may lead to a less significant reduction in the displacements and so the design concept to maximize the first mode damping ratio is chosen as the most efficient.
4) The increase in the first mode damping ratio was found to increase as the number of outriggers increases. The rate of increase is the highest when adding the first outrigger and the rate decreases with subsequent additions.
5) Simple design equations were proposed to estimate the optimal damper to connection stiffness ratio based on complex eigenvalue analysis. These equations estimate the approximate optimal damper-connection stiffness ratio that maximizes the first damping ratio in

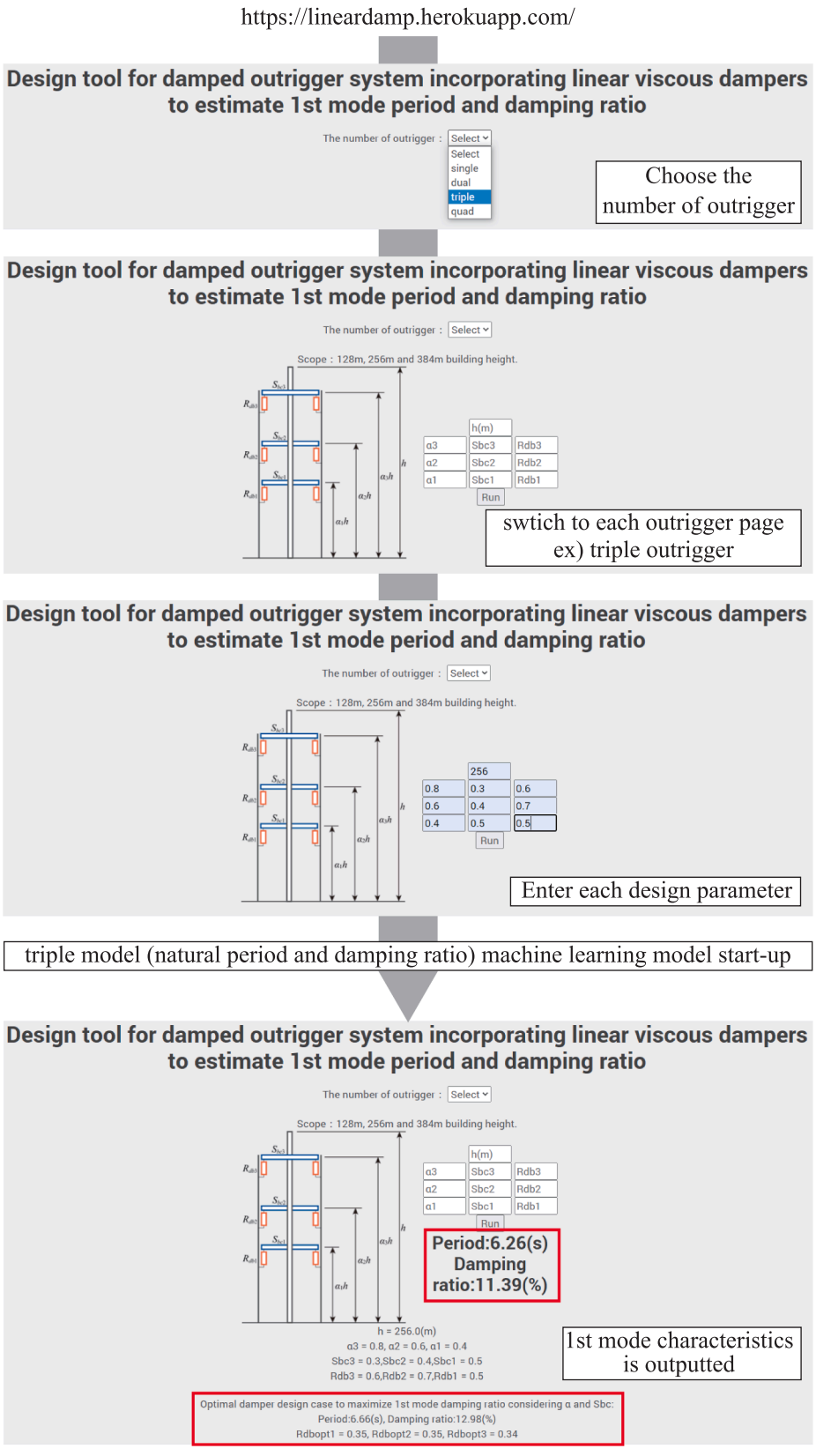

Fig. 29. Usage Instructions of the proposed design tool.

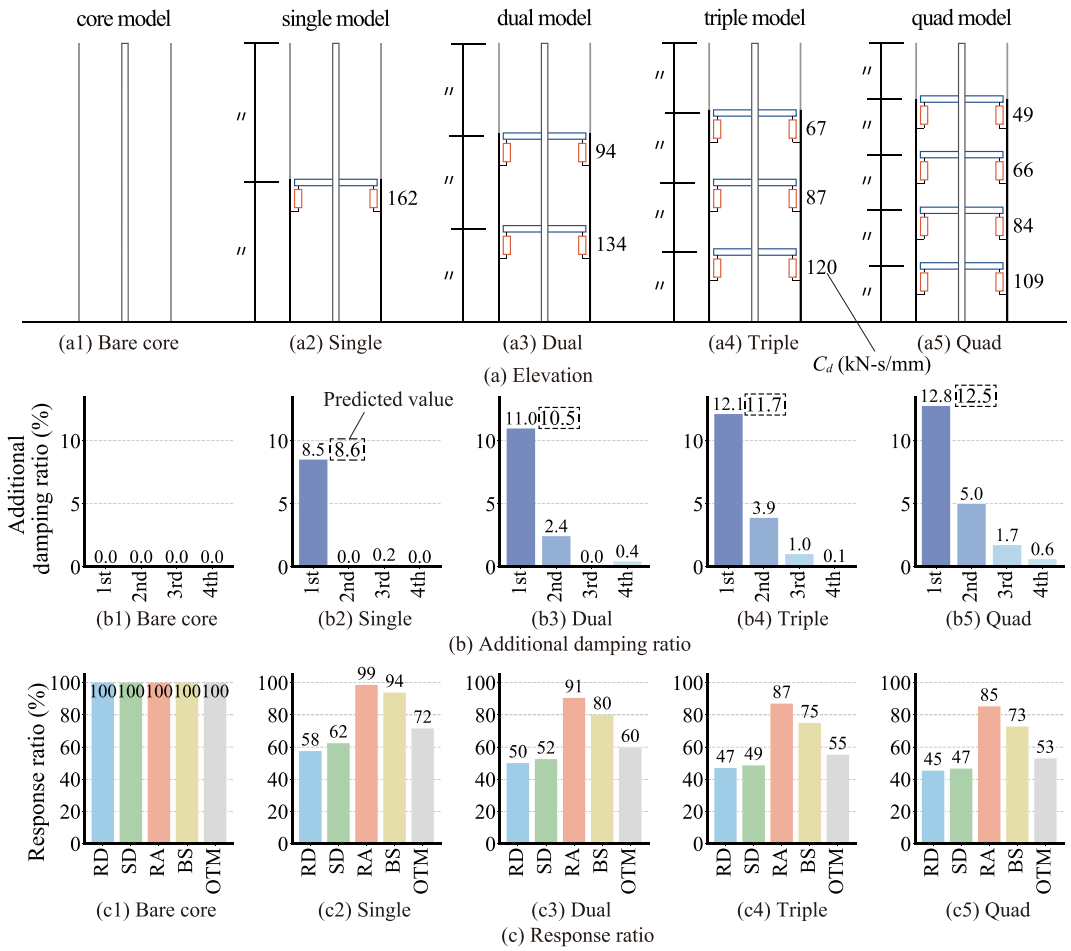

Fig. 30. Comparison of single to quad optimal models ($k_{t1\sim4} = 0.5 \times 10^6$ kN/m, 64-Story).

the specified range of the outrigger height ratio and connection (perimeter column + outrigger) to core stiffness ratio while allowing for flexibility in the outrigger height and stiffness of each element.

6) A machine learning model with the explanatory variables as the building height, $\alpha_{1\sim4}$, $S_{bc1\sim4}$, and $R_{db1\sim4}$, and the objective variables as the first mode natural period and first mode damping ratio was developed and the learning model was found to estimate the first mode characteristics of single to quad damped outrigger system with an accuracy of 95%.
7) An optimal design kit incorporating the design equations and the machine learning models was developed and distributed as a web application that may be used to estimate the primary damping ratio and optimally design the outriggers considering constraints such as the number of outriggers, damping coefficient, and outrigger height.

The web application-based optimal damper design tool presented in this study is currently only available for linear viscous damped outrigger systems, and expansion of the proposed simple design equations and machine learning models to include nonlinearity and other design earthquake levels may be areas of further study.

CRediT authorship contribution statement

Tomoki Asai: Investigation, Writing – original draft. **Yuki Terazawa:** Supervision, Conceptualization, Methodology, Investigation, Formal analysis, Writing – original draft, Writing – review & editing. **Takashi Miyazaki:** Methodology. **Pao-Chun Lin:** Writing – review. **Toru Takeuchi:** Supervision, Writing – review.

Declaration of Competing Interest

The authors declare that they have no known competing financial interests or personal relationships that could have appeared to influence the work reported in this paper.

Acknowledgement

The authors gratefully acknowledge the discussion about the optimal damper design procedure with Kazuma Goto and Ryota Tomioka from Arup Japan and Yasushi Ichikawa from Nippon Steel Engineering. The authors also appreciate the proof reading by Deepshikha Nair from Tokyo Institute of Technology. This work was supported by a research fund from the Japanese Society of Seismic Isolation (JSSI) and by a Grant-in-Aid from the Japan Society for the Promotion of Science Fellowships (No. 21K14288). A campus supercomputer (TSUBAME 3.0 at the Tokyo Institute of Technology) was used to develop the machine learning models.

References

[1] Smith S, Salim I. Parameter Study of Outrigger-Braced Tall Building Structures. J Struct Div, ASCE 1981;107(10):2001–14.
[2] Smith S, Coull A. Tall Building Structures: Analysis and Design, Chapter 14. John Wiley & Sons Inc; 1991.
[3] Smith RJ, Willford MR. The damped outrigger concept for tall buildings. Struct Des Tall Special Build 2007;16(4):501–17.
[4] Lago A, Trabucco D, Wood A. Damping Technologies for Tall Buildings Theory, Design Guidance and Case Studies. CTBUH: Elsiver Inc.; 2019.
[5] Smith R. The Damped Outrigger -Design and Implementation. Int J High-Rise Build 2016;5(1):63–70.

[6] Chen Y, McFarland D, Wang Z, Spencer B, Bergman L. Analysis of Tall Buildings with Damped Outriggers. J Struct Eng, ASCE 2010;136(11):1435–43.
[7] Deng K, Pan P, Lam A, Xue Y. A simplified model for analysis of high-rise buildings equipped with hysteresis damped outriggers. Struct Des Tall Special Build 2014;23 (15):1158–70.
[8] Zhou Ying, Xing Lili, Zhou Guangxin. Spectrum Analysis-Based Model for the Optimal Outrigger Location of High-Rise Buildings. J Earthquake Eng 2021;25(12): 2406–31.
[9] Tan Ping, Fang Chuangjie, Zhou Fulin. Dynamic characteristics of a novel damped outrigger system. Earthquake Eng Eng Vibrat 2014;13(2):293–304.
[10] Huang Bin, Takeuchi Toru. Dynamic Response Evaluation of Damped- Outrigger Systems with Various Heights. Earthquake Spectra 2017;33(2):665–85.
[11] Morales-Beltran M, Turan G, Dursun O, Nijsse R. Energy dissipation and performance assessment of double damped outriggers in tall buildings under strong earthquakes. Struct Des Tall Special Build 2018;28(1):e1554.
[12] Lin P-C, Takeuchi T, Matsui R. Seismic performance evaluation of single damped-outrigger system incorporating buckling- restrained braces. Earthquake Eng Struct Dyn 2018;47(12):2343–65.
[13] Lin Pao-Chun, Takeuchi Toru, Matsui Ryota. Optimal design of multiple damped-outrigger system incorporating buckling-restrained braces. Eng Struct 2019;194: 441–57.
[14] Terazawa Y, Asai T, Ishibashi S, Takeuchi T. Effect of design variables on dynamic response characteristic of single damped outrigger system incorporating linear viscous dampers. J Struct Construct Eng (Trans AIJ) 2020;85(774):1067–77 (in Japanese).
[15] Al-Furjan MSH, Habibi M, Ni J, Tounsi A. Frequency simulation of viscoelastic multi-phase reinforced fully symmetric systems. Eng Computers 2020.
[16] Rouabhia A, Abdelbaki C, Abdelmoumen AB, Fouad B, Houari H, Abdeldjebbar T, et al. Al-Zahrani: Physical Stability Response of a SLGS Resting on Viscoelastic Medium Using Nonlocal Integral First-Order Theory. Steel Compos Struct 2020;37 (6):695–709.
[17] Alimirzaei S, Mohammadimehr M, Abdelouahed T. Nonlinear Analysis of Viscoelastic Micro-Composite Beam with Geometrical Imperfection Using FEM: MSGT Electro-Magneto-Elastic Bending, Buckling and Vibration Solutions. Struct Eng Mech 2019;71(5):485–502.
[18] Takeuchi T, Wada A. Buckling-Restrained Braces and Applications. Jpn Soc Seismic Isolat 2017.
[19] Terazawa Y, Ishibashi S, Omura H, Asai T, Takeuchi T. Non-linear Dynamic Response Characteristic of Single-Damped Outrigger Systems with Oil Dampers or Elasto-plastic Dampers Considering Design Earthquake Levels. J Struct Construct Eng (Trans AIJ) 2022;87(791) [in Japanese, and accepted.].
[20] Terazawa Yuki, Takeuchi Toru. Generalized Response Spectrum Analysis for Structures with Dampers. Earthquake Spectra 2018;34(3):1459–79.
[21] Terazawa Yuki, Takeuchi Toru. Optimal damper design strategy for braced structures based on generalized response spectrum analysis. Jpn Arch Rev. 2019;2 (4):477–93.
[22] Sinha R, Igusa T. CQC and SRSS methods for non-classically damped structures. Earthquake Eng Struct Dyn 1995;24(4):615–9.
[23] The Japan Society of Seismic Isolation: Manual for Design and Construction of Passively - Controlled Building third Edition, Daioh Co., Ltd; 2013 (in Japanese).
[24] Ministerial Notification No. 1461 of the Ministry of Construction, Japan; 2000.
[25] The task committee of steel structure in AIJ: The state of art of Japanese seismic design of steel structures against large subduction zone earthquakes and large inland earthquakes, Document for the panel discussion of 2015 AIJ annual meeting, 2015.9 (in Japanese).
[26] https://github.com/optuna/optuna.